FULLERENE-OLIGOPHENYL MULTILAYERS GROWN BY HOT WALL EPITAXY

Diplomarbeit

zur Erlangung des akademischen Grades eines Diplomingenieurs in der Studienrichtung Technische Physik

eingereicht von
Gebhard Matt

angefertigt am Institut für Physikalische Chemie und Institut für Halbleiter- und Festkörperphysik an der Technisch-Naturwissenschaftlichen Fakultät der Johannes Kepler Universität Linz

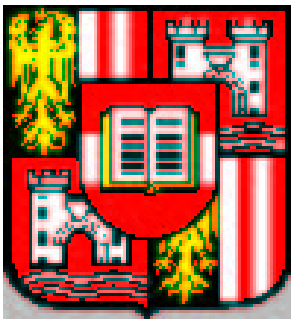

Betreuung: o.Univ.-Prof. Dr. N. S. Saricifci und
Linz, Juni 1999

Ich erkläre eidesstattlich, daß ich die vorliegende Diplomarbeit selbständig verfaßt und andere als die angegebenen Quellen und Hilfsmittel nicht benutzt habe. Diese Arbeit wurde bisher weder im Inland noch im Ausland in irgendeiner Form als Prüfungsarbeit vorgelegt. footnote-1

Gebhard Matt

Satz: LaTeX 2_ε

Thanks

First of all I want to thank my parents for supporting me all the years. Especially thanks to the whole group of our institute and the colleagues at the institute of solid-state physics. Particular I want to thank C. Brabec, H. Neugebauer, N.M. Tuan , W. Heiss and Dirk Badt from the institute of Biophysics. Also specially thank to all my friends who helped me having a great time at the university and at social events. Without the instructive advice of Prof. N.S. Saricifci and Prof. H. Sitter this work would have been impossible to carry out.

Gebhard Matt
Juni 1999

Ein Erfahrner weiß beim Singen
auch zur rechten Zeit zu enden;
gut ist's, zeitig aufzuhören,
kurze Lieder sind die schönsten,
- besser, sie zu Ende führen,
als den Faden zu verlieren.

– Kanteletar I 9

Contents

List of Figures

List of Tables

CHAPTER 1

Introduction

The excited electronic states of conjugated organic molecules have attracted interest since the early 1930, when the first theoretical approaches towards an understanding of the photophysical properties of large π-electron system were established. Besides the electronic levels of *isolated* molecules, molecular solid state properties have attracted many researchers and *molecular crystals* have been topics of numerous experimental and theoretical efforts. Over the last few years *thin films* of conjugated molecular systems have drawn considerable attentions to polymers as well as oligomeric materials, e.g oligo-thiophenes or oligo-phenylenes. These investigations were motivated by the possible technological applications, such as organic light emitting devices, field effect transistors and especially in our interests photovoltaic devices. In addition to the technological chances, there is still a need for deeper understanding of the thin film properties and among the various scientific questions the optical properties in the solid state are of fundamental interest. Model systems are therefore necessary to optimize the *growth* of thin organic films and to acquire *detailed* information on well-defined and ordered films, to establish a deeper understanding of the electronic properties.

The thermal stability of the used compounds para-hexaphenyl and C_{60} up to several hundred degrees, allows to use vacuum sublimation techniques like molecular beam epitaxy (MBE) or hot wall epitaxy (HWE). In this work Hot wall epitaxy method was applied for the preparation of thin organic films. The aim of this work was the controlled production of thin organic films and bi/multi-layer structures.

1. Conjugated Oligomers

Many small molecular semiconductors and unsubstituted oligomers take the form of rather rigid, planar molecules, which are generally insoluble in many organic solvents. Due their thermal stability, thin films of these low weight materials are achieved by sublimation techniques. Other advantages of oligomers compared to polymers are [**4**]:

- high molecular order (defect-free molecules)
- high chemical purity (up to electronic grade)
- high structural order in the solid state (up to single crystals)

On the other hand vacuum deposition is expensive and time-consuming, very cheap and fast preparation of thin film by spin-, drop-casting or offset-printing techniques are not directly (or so simple) applicable with these materials.

2. para-Hexaphenyl

The six member oligomer of para-poly-phenylene (PPP) namely para-hexaphenyl (PHP) [1] , is a organic semiconductor. It consists of a linear chain of six linked benzene (phenyl) rings showing strong delocalization in the direction of the chains, leading to a typical band-structure of a semiconductor with a bandgap ($\simeq$ 3eV). The strong delocalization of the π electron system yields in anisotropic electronic effects.

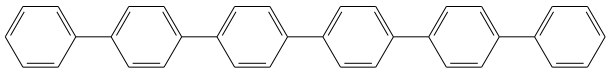

FIGURE 1.1. para-hexaphenyl (PHP)

In contrast to PPP has PHP a melting point of 437°Cand is thermally stable. It is insoluble in the most organic solvents. Other techniques like spin or drop-casting are not applicable with pure PHP. Due to its high photoluminescence quantum yield (above 30%) it is a promising candidate for active layers in light emitting diodes [**5**].

2.1. Crystal structure of PHP. The crystalline structure of PHP is monoclinic. This means that the lattice-constants of the conventional unit cell are not equal ($a \neq b \neq c$) and one angles between the axes not-equal 90°[**6**].

[1]the prefix stands for the position of the second phenyl ring. In organic chemistry the C-atoms are clockwise numbered in a phenyl-ring from 1-3 with the corresponding names ortho (1), meta (2) and para (3) this yields in a linear chain. Hexa (or Sexy) stands for six repeating units.

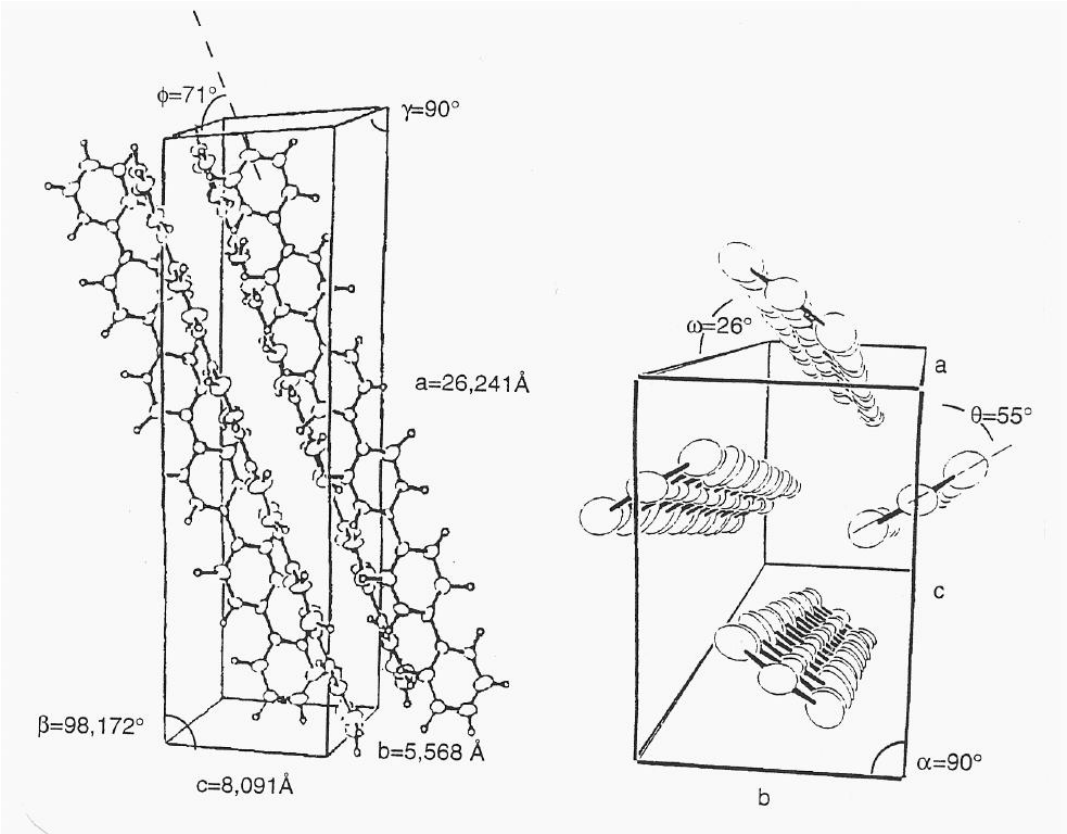

FIGURE 1.2. Orientation of PHP in the conventional unit cell

2.2. A simple model for the electronic structure of para-hexaphenyl. In this section, the Hueckel-method is applied for calculating a quasi-band-structure of PHP.

The MO energy level diagrams of π-electron molecules, especially of *conjugated systems* can be constructed using a set of approximations suggested by Erich Hueckel. These sp^2 de-localized orbitals spread over all the atoms and cannot be identified with a bond between a particular pair of atoms.

The Hueckel theory make the following simplifications:

- Separation from the π to the σ orbitals, and treat the latter as a rigid framework. In other words, forget the σ bonds except for the way that they determine the geometry of the molecule.
- Treat all C-atoms identical. This means that all the on site Coulomb-integrals α are set equal.[2]
- All Overlap-Integrals set equal to zero
- All resonance integrals between non-neighbors are set equal to zero to minimize the energy.
- All remaining resonance integrals are set equal (to β)[3]

[2]For example ethene, take the σ-bonds as given, and concentrate on finding the energies of the π bonds and its π-anti-bond

[3]these are obliviously very severe approximations, but they let us calculate at least a general picture of the MO energy levels with very little work

The ansatz is a linear combination of six benzene orbitals. The energy can be estimated with

$$E = \frac{\langle \Psi | H | \Psi \rangle}{\langle \Psi | \Psi \rangle} \tag{1}$$

By variation of eq.(1) gives a energy what is always higher than the realized one. The coefficients are found by setting all first partial derivatives equal zero to minimize the energy.

$$\frac{\partial E}{\partial c_i} = 0 \tag{2}$$

The linear combination of the six benzene π orbitals can be written as:

$$\Psi = \sum_{i=1}^{6} c_i p_i \tag{3}$$

Which yields for normalized p_i in:

$$\langle \Psi | \Psi \rangle = \sum_{i=1}^{6} c_i^2 + \sum_{i \neq j} c_i c_j \langle p_i | p_j \rangle \tag{4}$$

And for the numerator:

$$\langle \Psi | H | \Psi \rangle = \sum_{i=1}^{6} \alpha_i c_i^2 + \sum_{i \neq j} \beta_{i,j} c_i c_j \tag{5}$$

With the definitions $\alpha = \langle p_i | H | p_i \rangle$ and $\beta = \langle p_i | H | p_j \rangle$. In the literature α is called as Coulomb-Integral, β as Resonant-Integral and $\langle p_i | p_j \rangle$ as Overlap-Integral.

Hueckel approximation set $\alpha_i = \alpha$ (just identical C-atoms), $\beta_{i,i\pm1} = \beta$ and $\beta_{i,j\neq i\pm1} = 0$ (just neighbor atoms put in the calculation]

With eq.(5) and eq.(4) the variation of eq.(1) yields in an homogeneous equation-system. These can be written in the form:

$$\mathbf{D} = \begin{vmatrix} \alpha - E & \beta & 0 & 0 & 0 & 0 \\ \beta & \alpha - E & \beta & 0 & 0 & 0 \\ 0 & \beta & \alpha - E & \beta & 0 & 0 \\ 0 & 0 & \beta & \alpha - E & \beta & 0 \\ 0 & 0 & 0 & \beta & \alpha - E & \beta \\ 0 & 0 & 0 & 0 & \beta & \alpha - E \end{vmatrix} = 0 \tag{6}$$

These matrix has the roots:

$$E_n = \alpha + 2\beta \cos(\frac{n\pi}{7})]; \ (1 \leq n \leq 6) \tag{7}$$

Assuming electron-hole symmetry the energy can be described by "+" for the conducting band states and "−" for the valence band states. In the valence band all these eigenstate are occupied.

$$E_n = \pm[\Delta + 2\beta \cos(\frac{n\pi}{7})]; \ (1 \leq n \leq 6)] \tag{8}$$

The same calculation can bee done for the infinite system PPP (Para-Poly-Phenyl). In this case $\mathbf{D}$ eq.(6) is the same tridiagonal matrix just infinite large. A wave with the ansatz

$$s_n = e^{ipna} \tag{9}$$

is an eigenvector of determinate **D**. This can bee seen by looking at the n-element of **D**.

$$\begin{aligned}(\mathbf{D}s)_n &= \alpha s_n + \beta(s_{n-1} + s_{n+1}) = \\ &= [\alpha + \beta(e^{-ipa} + e^{ipa})]e^{ipna} = \\ &= (\alpha + 2\beta\cos(pa))s_n \end{aligned} \tag{10}$$

A eigenvalue of **D** in respect to s is $(\alpha + 2\beta cos(pa))$ p is a real number and has the physical interpretation of the momentum k and a is the distance between the benzene rings. For PPP they are $p_{min} = 0$ and $p_{max} = \pi/a$ yielding in a continuous spectrum.

$$E = \alpha + 2\beta\cos(a|k|);\ k = [0, \pi/a] \tag{11}$$

For PHP β is set to -1.16eV [**7**] and Δ is set to 3.63eV. Similar calculation on the benzene molecule yields in four different energy-levels. The two lowest are completely occupied. Denoted as a_{2u}^2, e_{1g}^4 [**8**]. The two times degenerated level $e_{1g}\pi$ is called the highest occupied molecular orbital (HOMO). On PHP one of these level are characterized by a high electron density at the carbon atom, which are a part of the C−C bridge between the rings and these benzene orbitals are spread across the whole molecule forming de-localized states with energies given by eq.(8). The other one has a node at the bridge to next benzene ring and the low orbital overlap results in the formation of non-bonding dispersionsless PHP states. Similar considerations can be applied to the benzene $e_{2u}\pi^\star$ states. In the ansatz the linear combination of the π orbitals are one of the e_{1g} benzene orbitals.

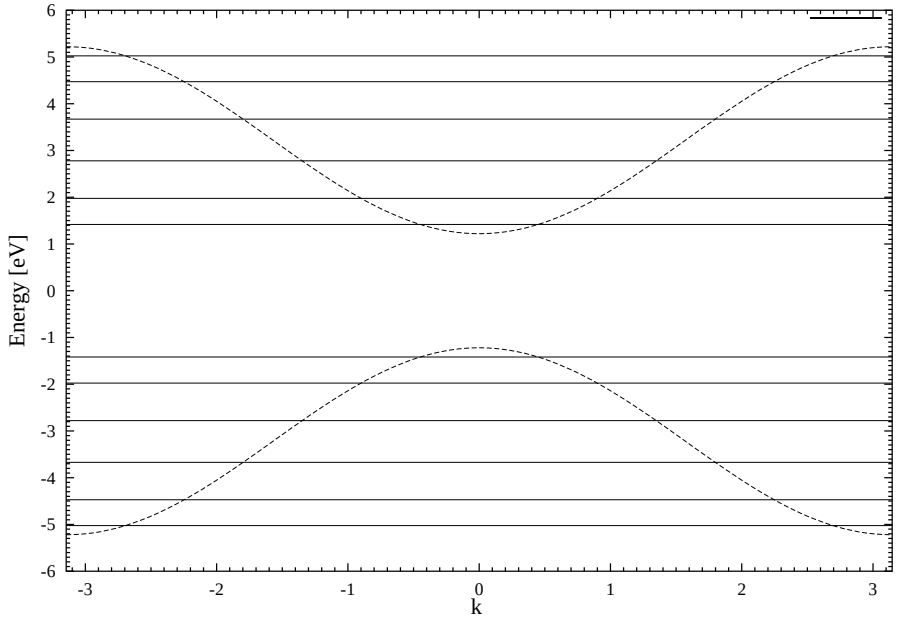

FIGURE 1.3. Band-structure PPP drawn as cosine-function and the energy-levels in PHP drawn as lines

2.3. Optical transitions. Luminescence studies shows for different excitation directions anisotropy optical absorption. These effects can be understood by applying elementary selection rules. The transmission between Ψ and $\Psi^\star$ are just

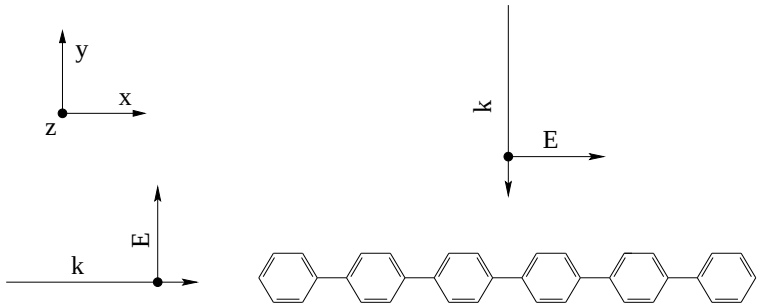

FIGURE 1.4. PHP-molecules under different excitation direction. See text.

allowed if the orbitals have different parity or the integral eq.12 does not vanish. In first order of 'disturbing' theory, the Hamilton is separated in $H = H_{molecule} + H_1$ where $H_1 = e\mathbf{rE}$ is the linear disturbing-term from the excitation-light. An absorption can be measured if the integral eq.12 does not vanish

$$\langle \Psi^\star | eEr | \Psi \rangle \neq 0 \tag{12}$$

This can just be valid if the Ψ and $\Psi^\star$ have different parity. The eigenstates of the Parity-operator P are $P|\pi\rangle = (-1)^n|\pi\rangle$ where n is even/odd for even/odd wavefunctions. By applying $PrP = -r$ in eq.(12)

$$\begin{aligned} \langle \Psi^\star | e\mathbf{Er} | \Psi \rangle = \\ -eE_\parallel \langle \Psi^\star | PrP | \Psi \rangle = \\ (-1)^{n^\star+n+1} \langle \Psi^\star | e\mathbf{Er} | \Psi \rangle \end{aligned} \tag{13}$$

And this is just valid if $n + n^\star$ is odd or in other words Ψ and $\Psi^\star$ have a different parity [4]. By defining the wavefunction as product of separated wavefunctions in x and y/z coordinates $\Psi = \Psi_x \Psi_{yz}$ the allowed transitions by applying E in x (or y/z) direction is given by $\langle \Psi_x^\star \Psi_{yz}^\star | PxP | \Psi_x \Psi_{yz} \rangle = \langle \Psi_x^\star \Psi_{yz}^\star | x | \Psi_x \Psi_{yz} \rangle (-1)^{n_x^\star + n_x + 1}$. And require different parity of Ψ in the direction of E. For different excitation direction we can conclude:

- E vector is in $z-y$ plane: In in $z-y$ plane (see fig.1.4) the parity between Ψ_{yz} to $\Psi_{yz}^\star$ is changing and this yields in dipole allowed transitions from HOMO to LUMO and HOMO-1 to LUMO+1 respectively
- E vector is in x-direction: In eq.8 electron/hole symmetry is assumed [5] and the symmetry of the wavefunction in HOMO/LUMO, HOMO-1/LUMO+1,...are the same. This yields in forbidden transitions from HOMO to LUMO and HOMO-1 to LUMO+1 respectively

[4] such transitions are called "dipole-allowed"

[5] this can be done, because the Fermi-level is close to middle of the bandgap [**9**]

2.4. Influence of linear absorption versus chain length. The linear absorption and emission of oligomers shifts to lower energies for longer chain lengths in an approximately linear relation with the inverts number of the monomer units [**10**]. In the limit of infinite long chain e.g. PPP become these approximation unreliable and the non-linearity on the reciprocal conjugation length can be described by [**11**].

$$E = A + B(1/n) + C(1/n^2) \tag{14}$$

Where n is the number of the monomers. These "fit" can bee understood by expanding the cosine function in eq.8 to the second order and this is in agreement with measurements in [**12**].

CHAPTER 2

Photo excitation and electron transfer

In this chapter general considerations of photo-excitation on conjugated polymers/oligomers are presented. In the text we are discussing in termini of conjugated polymers. Similar concepts can be applied to the short member of polymers called oligomers.

The discovery of semiconducting, conjugated polymers and the ability to dope these over the full range from insulator to metal resulted in the creation of a class of new materials that combines the electronic and optical properties of semiconductors and metals with the attractive mechanical properties and processing advantages of these polymers. Many conjugated polymers in their un-doped, semiconducting state are electron donors upon photo-excitation (electrons promoted to the anti-bonding $\pi^\star$ band). The possibility to utilize light absorbing systems to duplicate the overall process of photosynthesis is attracting more and more researchers in the scientific community. Conjugated systems seem to fulfill all properties required for photosynthesis: light absorption and charge separation. The idea of using this property in conjunction with a molecular electron acceptor to achieve long living charge separation was based on the stability of the photo-excitations (such as polarons or polaron pairs) on the conjugated-system backbone. After the transfer of the photo-excited electron to an acceptor unit, the resulting cation radical (positive polaron) species on the conjugated-system is stabilized due to the delocalization of the excitation over several repeating units. In analogy to the chemical doping process, we will describe the photoinduced electron transfer as "photo-doping ". A basic description of the intermolecular electron transfer between a donor D and an acceptor A is given as follow:

(1) Step: $\mathsf{D} + \mathsf{A} \rightarrow {}^{1,3}\mathsf{D}^\star + \mathsf{A}$, (excitation on D)
(2) Step : ${}^{1,3}\mathsf{D}^\star + \mathsf{A} \rightarrow {}^{1,3}(\mathsf{D}-\mathsf{A})^\star$, (excitation delocalized on D-A complex)
(3) Step : ${}^{1,3}(\mathsf{D}-\mathsf{A})^\star \rightarrow {}^{1,3}(\mathsf{D}^{\delta^+} - \mathsf{A}^{\delta^-})^\star$, (charge transfer initiated)
(4) Step : ${}^{1,3}(\mathsf{D}^{\delta^+} - \mathsf{A}^{\delta^-})^\star \rightarrow {}^{1,3}(\mathsf{D}^{+\bullet} - \mathsf{A}^{-\bullet})^\star$, (ion radical pair formed)
(5) Step : ${}^{1,3}(\mathsf{D}^{+\bullet} - \mathsf{A}^{-\bullet})^\star \rightarrow \mathsf{D}^{+\bullet} + \mathsf{A}^{-\bullet}$, (charge separation)

Here 1 and 3 denote the singlet or triplet state respectively. Steps 1 and 2 describe the photo-excitation of the conjugated system (donor) and the delocalization of the excitation to a near acceptor. The acceptors can be either covalently bound (intramolecular electron transfer) or spatially very close located (intermolecular electron transfer). At each step, the D-A complex can relax back to the ground state of the single components either by energy deficient processes to the lattice (heating) or through radiation. The critical step for the charge transfer, step 4, is influenced by a number of factors. Generally, the ionization potential of the excited state of the donor ($I_{\mathsf{D}^\star}$), the electron affinity of the acceptor (A_{A}) and the Coulomb attraction of the separated radicals (U_C) including the polarization effects should match the following inequality:

$$I_{\mathsf{D}^\star} - A_{\mathsf{A}} - U_C \leq 0 \tag{15}$$

But even when this criterium is fulfilled, some other factors may inhibit the charge transfer process such as a potential barrier preventing the separation of the photo-excited electron-hole pair or the morphology of the blend preventing the overlap of the donor and acceptor excited state wave functions due to too large intermolecular spacings. Independently, Santa Barbara and Osaka groups reported studies on the photophysics of mixtures and bilayers of conjugated polymers with fullerenes [**13, 14, 15, 16, 17, 18, 19, 20, 21**] The experiments clearly evidenced an ultrafast, reversible, metastable photoinduced electron transfer from conjugated polymers onto the C_{60} in solid films. Schematic description of this phenomenon is displayed in fig.2.1

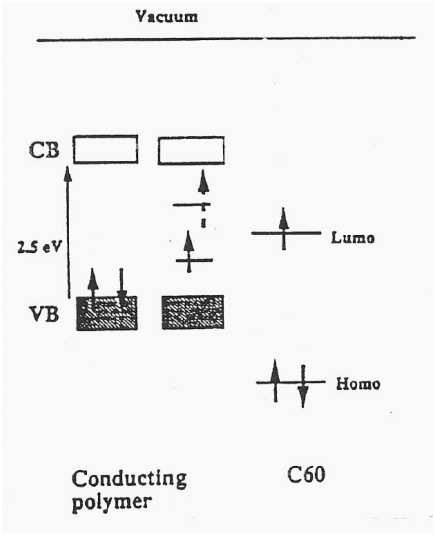

FIGURE 2.1. Schematic description of the photoinduced electron transfer

1. The photophysics of conjugated Polymers/C_{60}composites

A strong quenching of the luminescence in the present of C_{60} of a wide class of conjugated polymers [**18, 21**] is consistent with efficient ultrafast photoinduced electron transfer. The occurrence of luminescence quenching can be explained by various mechanisms. The excited singlet state can relax to the ground state also by non-radiative processes (thermal heating), energy transfer of electron transfer processes. Since the absorption and luminescence studies demonstrate that the excited states of the conjugated polymers strongly interact with C_{60}, a comparative spectroscopic study of this excited state is necessary. The first results on the excited state spectroscopy of these composites originate from near-steady-state photoinduced absorption (PIA) studies. To clearly distinguish the spin multiplicity of the photoinduced absorption (PIA) peaks, photoinduced absorption detected magnetic resonance experiments were performed [**17**].

1.1. Steady State Infrared Photoinduced Absorption. In semiconducting, conjugated polymers, the quasi-one-dimensional electronic structure is strongly coupled to the chemical (geometrical) structure. As a result, the nonlinear excitations (solitons, polarons and polaron pairs) are dressed with local structural distortions creating states with energies within the energy gap. "New" infrared

bands with large intensities (IRAV modes) are induced by doping and/or photoexcitation. Solitons, polarons and polaron pairs are charged "defects" which break the local symmetry and therefore make Raman modes infrared active [**22, 23, 24**]

1.2. Direct Experimental Observation of the Metastable Charge Separation: Light Induced Electron Spin Resonance (LESR). A powerful method to investigate charge transfer systems are light induced Electron Spin Resonance studies (LESR). Definitive evidence of charge transfer and charge separation is obtained from these experiments. Two photoinduced ESR signals can be resolved; one at g=2.003 and the other at g=1.9997 [**13**]. The higher g-value line. is assigned to the conjugated polymer cation (polaron) and the lower g-value line to C_{60}-anion. The assignment of the lower g-value line to C_{60}- is unambiguous, for this low g-value is atypical for organic systems [**25, 26**]; the higher g-value is typical of conjugated polymers. At 200 K, the LESR signals of the different specimens have nearly vanished, demonstrating the reversibility of the photoinduced generation of radicals. Subsequent LESR measurement cycles of heating to 290K, cooling down to 100K, illumination with light, switching light off and heating up again yield identical results. Lately [**27, 28**] the saturation behavior and the line shape of the LESR signal of conjugated polymer/C_{60} systems has been studied. Analysis confirms the finding that the two different peaks belong to different light induced radicals.

1.3. Photovoltaic and Photodetector applications. The utilization of organic materials for photovoltaic devices has been investigated intensely during the last couple of decades (for a summary of the early reports see for example [**24, 29, 30**] Tang demonstrated photovoltaic activity in small molecular bilayers that were vacuum evaporated [**31**]. Extensive literature exists on the fabrication of solar cells based on small molecule dyes as well as donor-acceptor systems (see for example [**32**] and references therein). Inorganic oxide semiconductors have also been used to facilitate electron transfer from organic dyes to achieve charge separation and photovoltaic conversion (see for example [**33, 34**] and references therein). With the improvement and development in the synthesis of soluble conjugated polymers, conjugated polymer layers have been used in solar cells (see for example [**35, 36, 37**] and references therein). Even the acceptor properties of fullerenes have been utilized for photodiodes, although not with conjugated polymers. Yamashita and coworkers reported a bilayer photodiode based on the organic donor tetratiafulvalene (TTF) and C_{60} [**38**].

Because of the ultrafast photoinduced electron transfer with long lived charge separation, the conjugated polymer/C_{60} system offers a special opportunity. Using conjugated polymers as donors with different acceptors, results in photoinduced charge separation with quantum efficiency near unity and with correspondingly enhanced device performance.

CHAPTER 3

Hot Wall Epitaxy

The growth technique used in this work is the Hot Wall epitaxy (HWE). The HWE method was developed by Lopez Otero [**39**] at university of Linz (Austria) for deposition of IV-VI compounds. In contrast to other vacuum sublimation techniques like MBE, HWE growth was performed in high vacuum conditions. HWE allows to grow epilayers close to the thermodynamic equilibrium. Detailed description of the HWE technique and of the used HWE-setup are given in [**2**] and [**40**].

The HWE system is, in contrast to other growth techniques like flash evaporation or more sophisticated MBE methods, a closed growth system [**40**]: The HWE system, as depicted in [**1**] and depicted in fig.3.1, consists of a quartz tube which serves as growth reactor. There are at least four separate heaters allowing the independent temperature adjustment in four regions. At the bottom of the tube the source material is evaporated at a temperature T_{Source}. The substrate is placed close to the tube end (distance 5mm) and can be heated during the growing process (temperature T_S). The region between source and substrate (temperature T_{Wall}) guarantees a nearly uniform and isotropic flux intensity and kinetic energy of the molecules. Finally, the main advantages of the HWE growth technique are:

- HWE works close to the thermodynamic equilibrium, which is very essential in the case of van der Waals epitaxy of organic compounds
- The loss of evaporating material is reduced to a minimum
- The high vapor pressure of the source material can be maintained and the grow rate can be controlled in a wide range
- Only high vacuum technology is required

Also the disadvantage can be summarize as:

- The in-situ control of the growing process is more complicated compared to other sublimation methods

1. HWE-setup

In fig.3.2 the used HWE setup is shown. It consists of two growth reactors and one annealing/pre-heating oven. The sample can be moved with a step-motor from one oven to the other one. This allows the production of multilayer-structures. The high-vacuum valve is installed between the growth chamber and the Load lock chamber. This allows the change of the substrate without braking the vacuum in the growth chamber. If necessary to prevent the sample from air, it can be taken to the measurements under vacuum conditions by removing a part of the load lock chamber (see [**40**] for details).

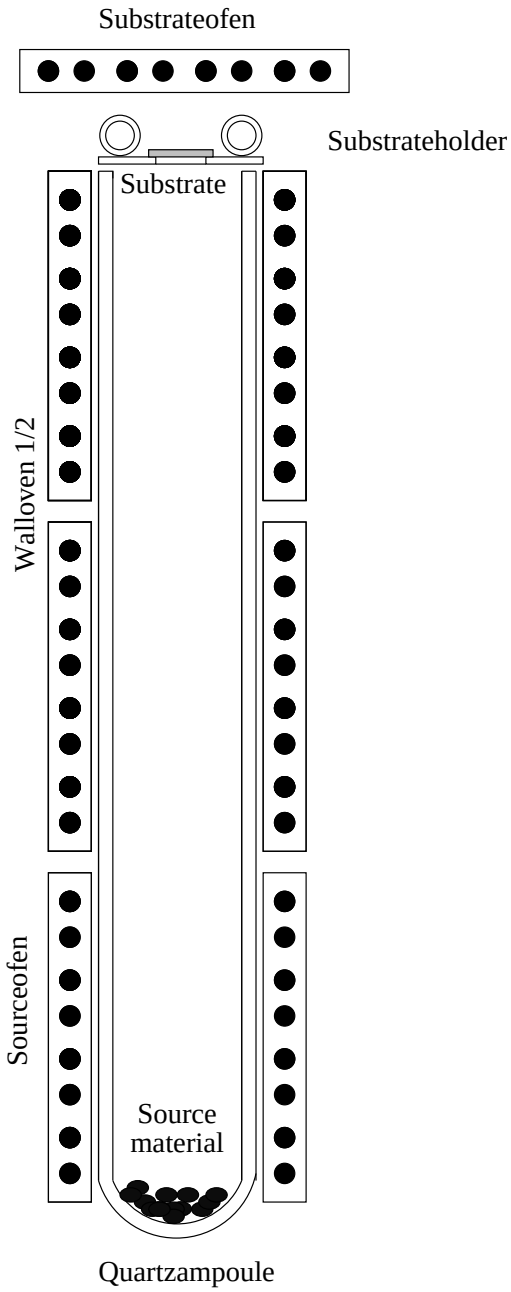

FIGURE 3.1. Schematic cross section of Hot Wall Epitaxy system

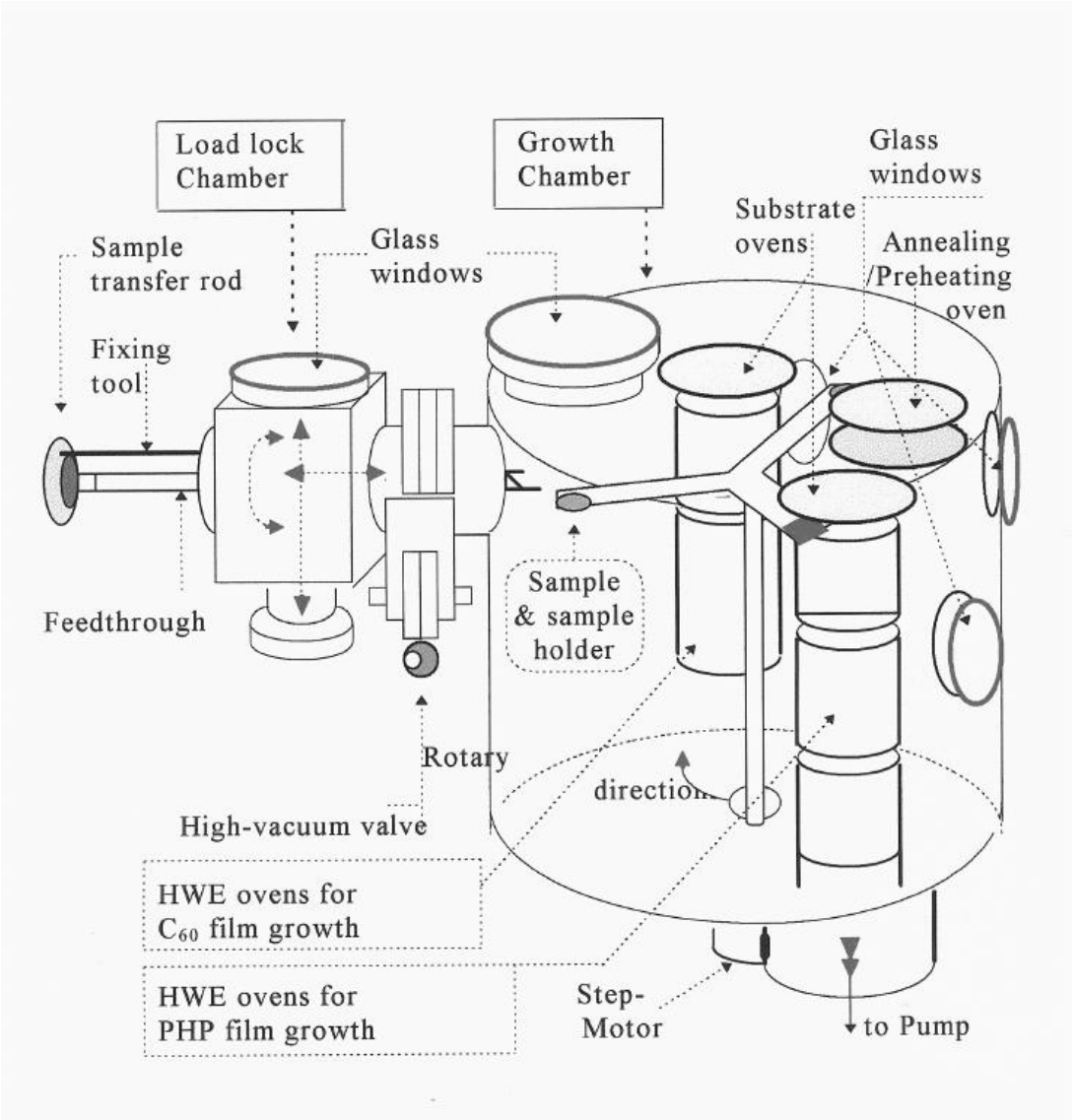

FIGURE 3.2. Hot Wall-Epitaxy apparatus for PHP/C_{60} film growth. There are two hot wall systems and one annealing/preheating oven in growth chamber

2. Growth of pristine C_{60} films on mica substrates

The C_{60} films were mostly grown on (001)-oriented cleaved mica. It was proven that mica is a promising substrate for the growth of thin C_{60} films of high crystalline quality with a lattice mismatch of about 3.4 % [**1, 2, 40, 41**]. In fig.3.3 a schematic picture of a C_{60} monolayer on mica is given. In this work, all C_{60} films on cleaved mica (100) were grown with the optimized parameters given in [**1**] resulting in mono-crystalline C_{60} films. The growth conditions were: T_S=140° , T_{Wall}=400°, T_{Source}=400°. Resulting in a low deposition rate of ≃2 nm/min

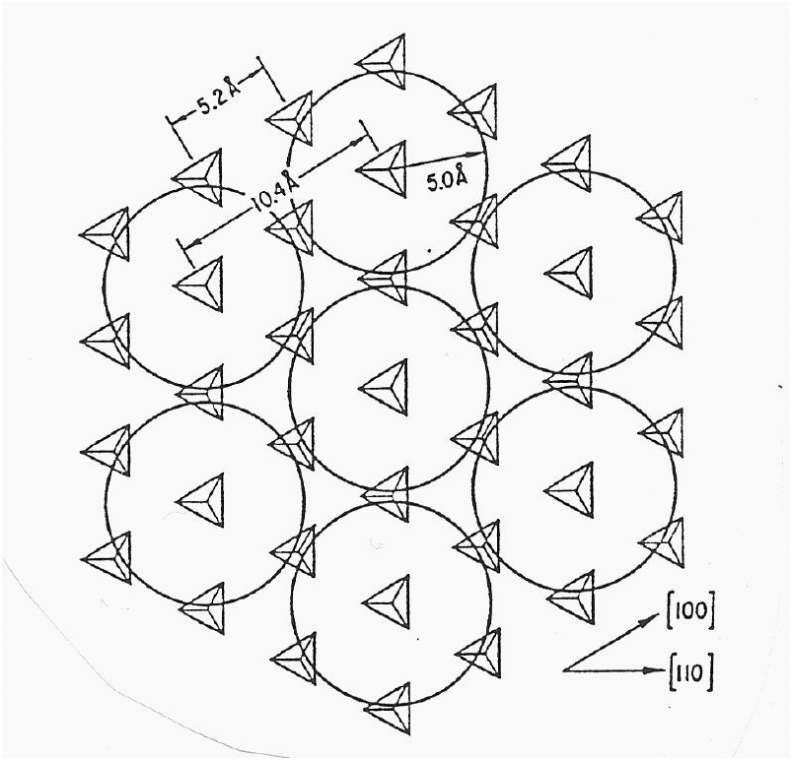

FIGURE 3.3. Schematic picture of a C_{60} monolayer on mica. The C_{60} molecules are drawn as circles. The mica silicontetraeder are drawn as triangles (Just each second silicon triangle is drawn). Taken from ref.[**1**].

3. Sample preparation

The enemy of every epitaxy-method is dirt. Very careful sample-preparation is essential. After cleaning the substrates were put immediately in the load lock-chamber. The used substrate-materials were:

- glass with a high quality surface
- gold coated glass: glass was coated with a thin highly conduction transparent gold layer.
- ITO-coated glass: Indium-Tin-Oxid (ITO) sputtered glass. ITO is conductive and highly transparent.
- Mica: Muscovite mica; crystalline substrate. Very promising substrate-material for production of thin organic films with remarkable high crystalline quality. Figure 3.4 present a typical C_{60} rocking curve on mica.

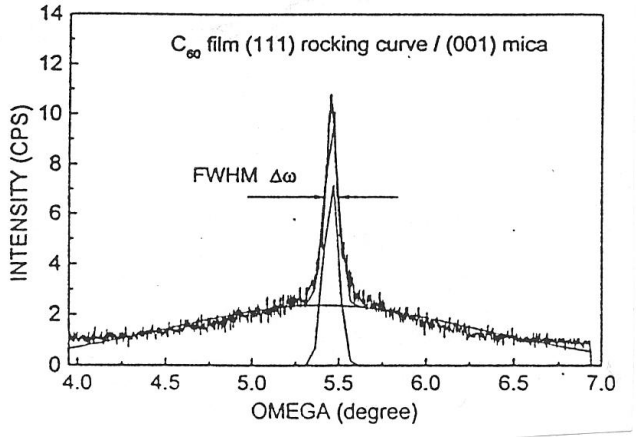

FIGURE 3.4. Rocking curve of a typical C_{60} film on [001] mica. Taken from ref.[**2**].

3.1. Preparation of glass, gold coated glass and ITO substrates. For the cleaning procedure just solvents from high chemical grade and diionized water was used. The cleaning process included the following steps:

- removing of fingerprints etc. with rinsing agent
- "mechanical" rubbing of the substrate with Kodak-paper and Acetone

Repeating of the two first steps several times. In the next steps a strong ultra-sonic bath with heating was used. Each cleaning step with the ultra-sonic takes around 10 min. Between each step nitrogen blowing was used to remove the solvents.

- Methanol (2 times)
- Acetone (3 times)
- Trichloroethylene (2 times)

3.2. Preparation of mica substrates. [001] oriented Muscovite mica can be very easily cleaved with a scotch-tape to get a clean surface. It is important to remove the tape in a small angle parallel to the substrate to get a perfect cleaved surface. Large steps on the mica surface disturb the growth process.

4. Preparation of thin PHP films

The first growth experiment was done on glass substrates to find the necessary growth conditions. The growth process itself is described in other sections. At all growth experiments the wall-temperature T_{Wall} was set equal to the source temperature T_{Source} and the pre-heating-oven temperature was set equal to the substrate-oven temperature to minimize the variation of the growth parameter. The pre-heating time was set to 30 min, to be sure that the substrate reaches the preheat-oven temperature. At this point it is necessary to note, that further variation of the growth-parameters are required -like variation of the deposition-rate, film-annealing...etc.

4.1. Variation of the Source-temperature. In fig.3.5 the Arrhenius-plot of the deposition rate versus the source-temperature is presented. In Arrhenius

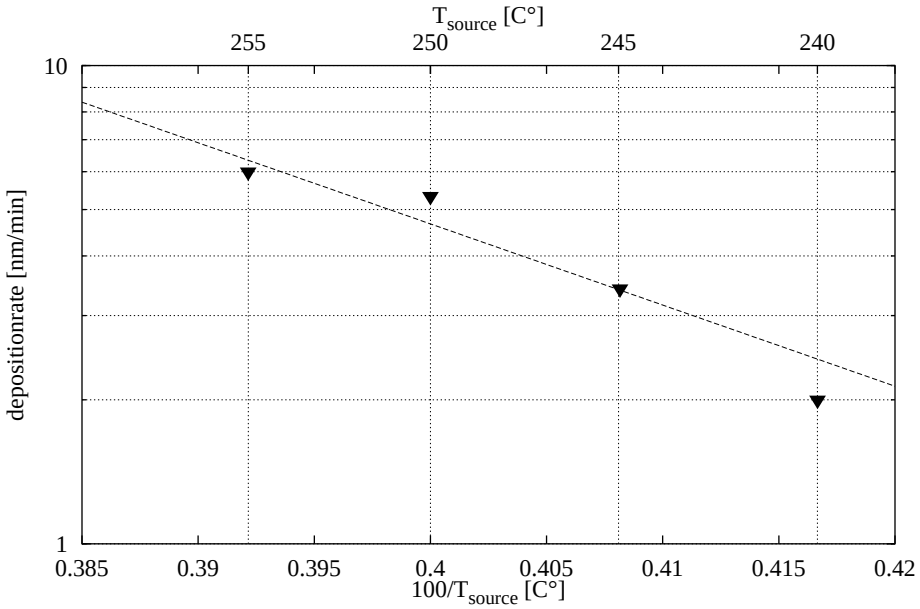

FIGURE 3.5. Arrhenius plot of deposition-rate in [nm/min] of PHP on glass versus T_{Source}, T_S=100°, growing time=60 min.

presentation the measured point are aligned a long a line which allows to write [**42**]:

$$Rate = const. * e^{-\frac{E_a}{kT_{Source}}} \tag{16}$$

Assuming that the deposition-rate is proportional to the flux-rate of the PHP molecules, E_a corresponds to an "activation-energy" and has the value $E_a = 3907/k_B = 0.18eV$.

4.2. Variation of the growth time. In fig.3.6 the film-thickness of PHP on glass versus the growth-time at two different substrate-temperatures is presented. The source temperature T_{Source} was 240°in both cases. The resulting deposition rates at T_S=100°and 140°are 2 and 2.3 nm/min respectively.

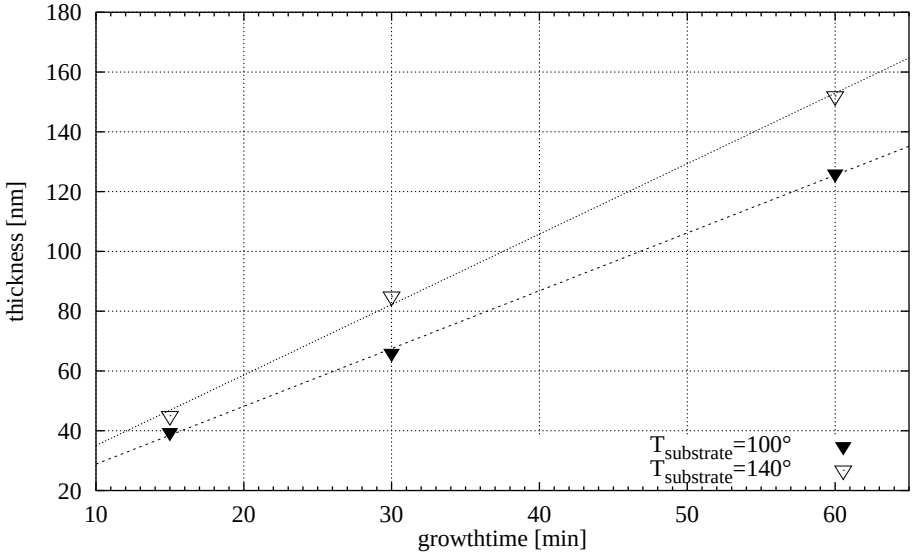

FIGURE 3.6. Film thickness versus growth time

CHAPTER 4

Results and discussions

1. Morphology studies

In this chapter the results of AFM and Light-microscope-studies are presented. The given pictures are not selected areas of the samples. At all samples PHP was homogeneously distributed over the hole substrate and no significant change of the morphology at different positions was observed.

1.1. Light microscope studies of PHP and PHP/C_{60} bilayer. Observations are a good technique to get a first impression of the film morphology.

Table.4.0 gives the growth parameters of samples used for light microscope pictures. The pictures were taken in trough-light and on-light geometry respectively. In trough-light the incident light was polarized and a second polarizer in the ocular was used as analyzer. In on-light geometry the unpolarized foci-sized light from a halogen lamp illuminated the film under a small angle of 10°.

TABLE 4.0. Growth parameter of PHP and PHP/C_{60} bilayer on mica

Sample-Nr.	T_S [°C]	PHP $T_{Wall/Source}$ [°C]	C_{60} $T_{Wall/Source}$ [°C]	PHP/C_{60} Growth time [min]	Preheat [°C]	Ref Fig.
mcp04	140	240	400	20/60	140	4.3,4.4
mc05	90	240	-	20/-	90	4.1,4.2
mcp06	140	240	400	20/20	140	4.5
mcp07	90	240	400	20/20	90	4.6

1.1.1. *Light-microscope studies of PHP on mica.* In this section light-microscope pictures of PHP on mica are given.

As proven with the AFM-microscope PHP on mica is forming large oriented structures like "needles". Is the growth process not distorted by e.g step on mica surface the orientation of the needles do not change. Such perfect cleaved mica surfaces are possible to prepare [1].

Fig. 4.1,4.2 was shot in on-light geometry. The incident beam come from the right side parallel to the horizontal border of the picture. Is the incident beam acting perpendicular to the "needles", diffracted light is observed (fig. 4.1). No non-reflective areas except one edge was observed. After rotating the sample mc05 120° clockwise, these edge begin to diffract the incident light. As can be seen on the AFM picture fig.4.21 a step on the mica surface distorted the PHP film growth process and turned the direction of the needles.

[1] see caption **Substrate preparation** on page 14

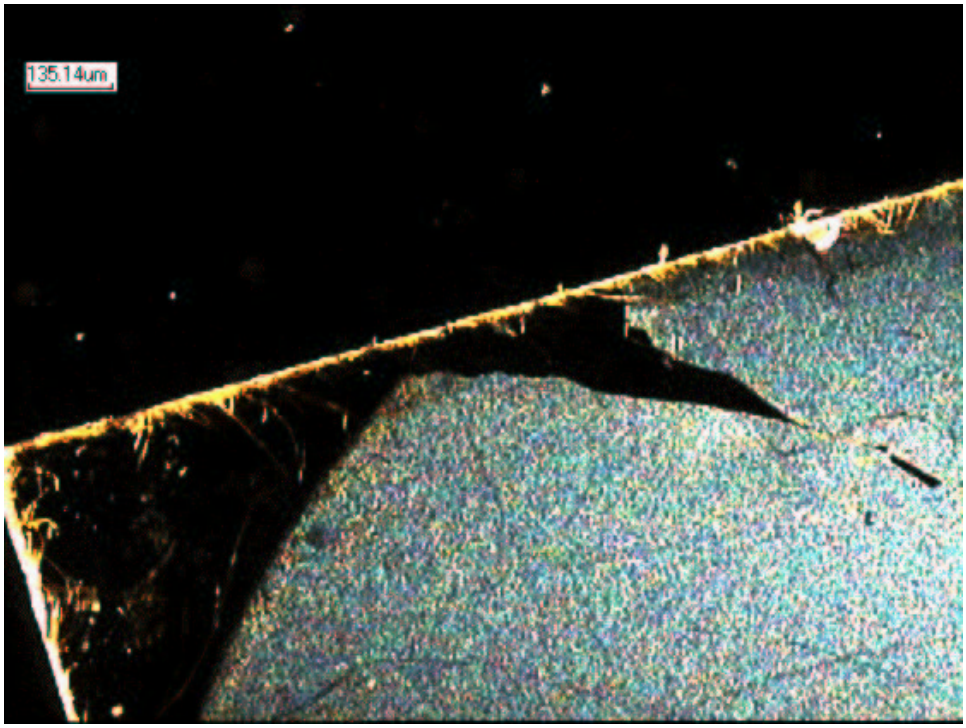

FIGURE 4.1. Sample mc05: Light microscope picture of PHP on mica in on-light geometry.

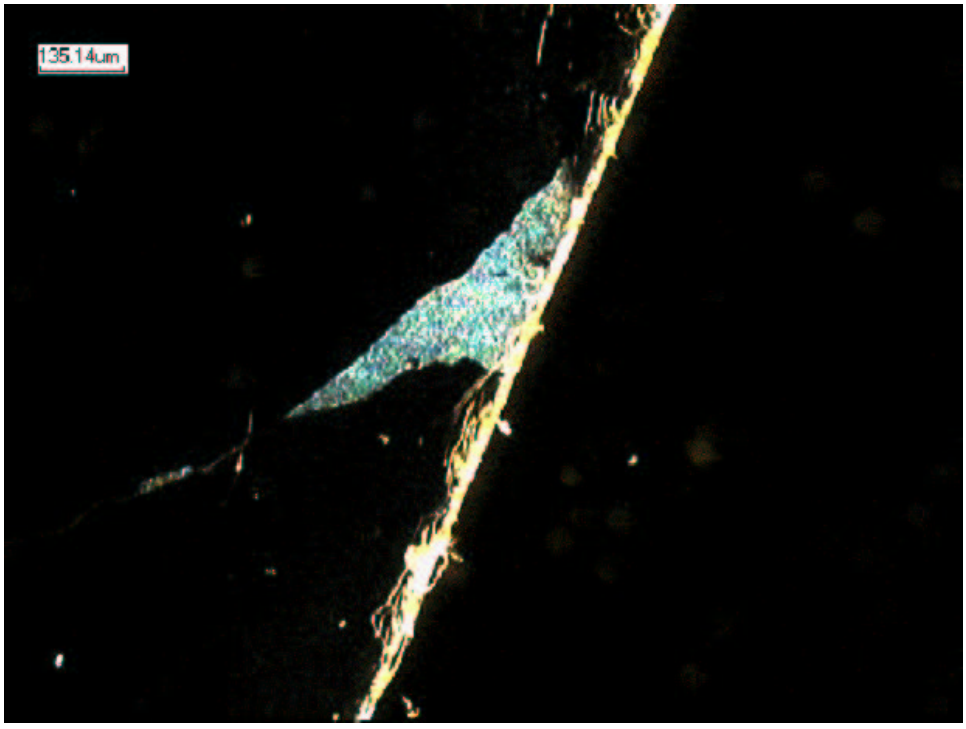

FIGURE 4.2. Sample mc05: Light microscope picture of PHP on mica in on-light geometry. Rotated 120°in respect to fig.4.1

1.1.2. *Light-microscope studies on C_{60}/PHP bi-layer on mica.* In this section light-microscope pictures of bilayers on mica are represented. Fig.4.3 and fig.4.4 shows photos from the same area of the sample mcp04. Fig.4.3 was shot in on-light and fig.4.4 was shot in trough-light geometry. In on-light geometry different bright areas of diffracted light are detected. In trough-light geometry a unequivocal relation to the different bright areas in fig.4.4 and the diffracted light in fig.4.3 can bee seen. As proven with the AFM microscope at high T_S PHP is forming oriented island on C_{60} films (see fig.4.28). This indicates the different orientation of the PHP-islands on C_{60} coated mica.

The brown area in fig.4.4 is pure C_{60} (both layers are not exactly at the same position on the substrate). In fig.4.6 and fig.4.5 two light-microscope pictures of sample mcp06 and mcp07 grown at T_S=90° and 140° are given.

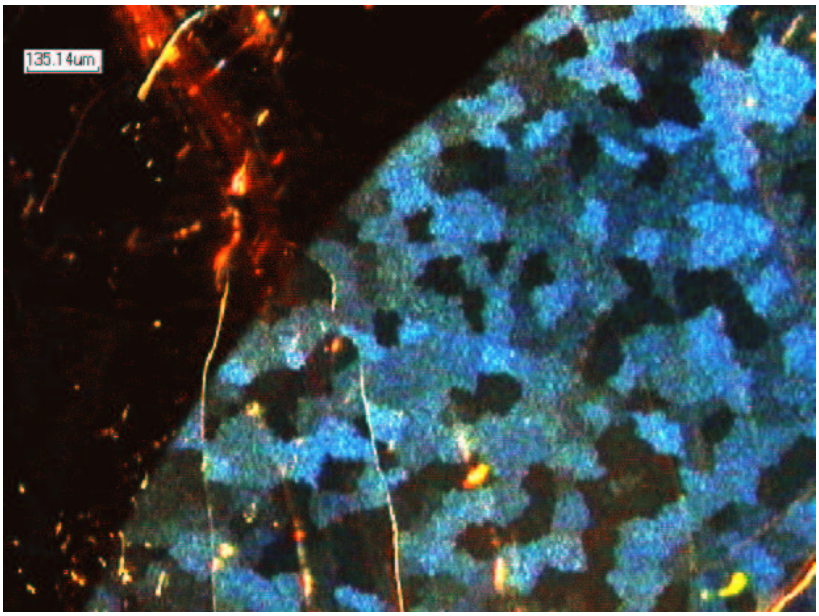

FIGURE 4.3. Sample mcp4: Light microscope picture of PHP/C_{60} bilayer on mica in on-light geometry.

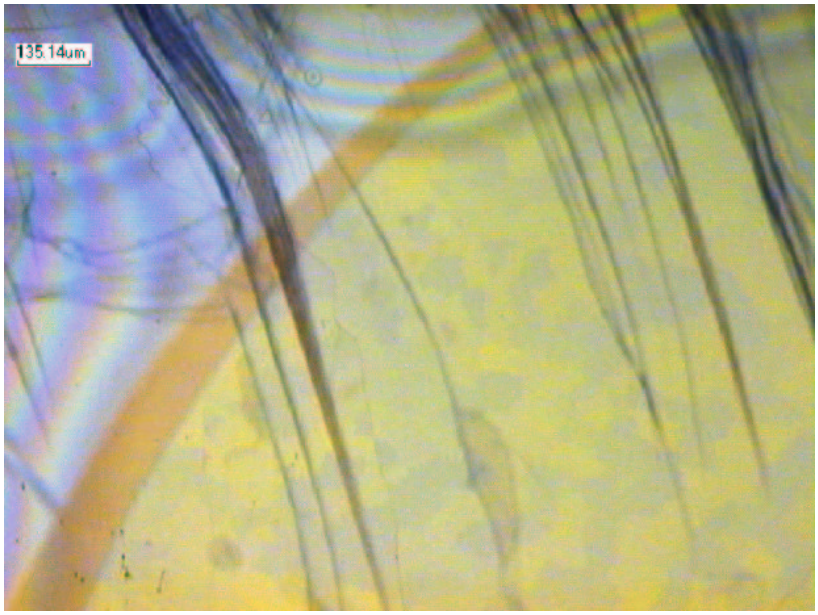

FIGURE 4.4. Sample mcp4: Light microscope picture of PHP/C_{60} bilayer on mica in trough-light geometry.

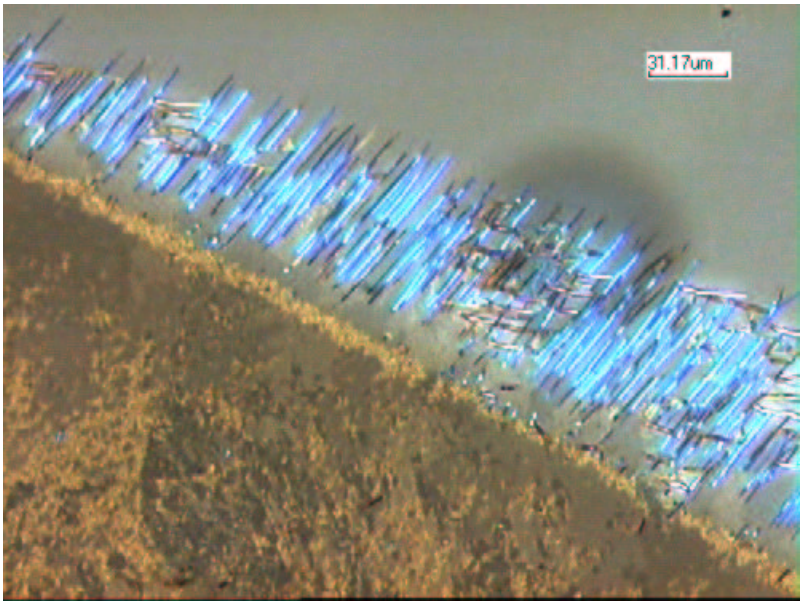

FIGURE 4.5. Sample mcp06: Light microscope picture of C_{60}/PHP bilayer on mica in trough-light geometry. Blue:PHP, brown C_{60}/PHP. T_S=140°C

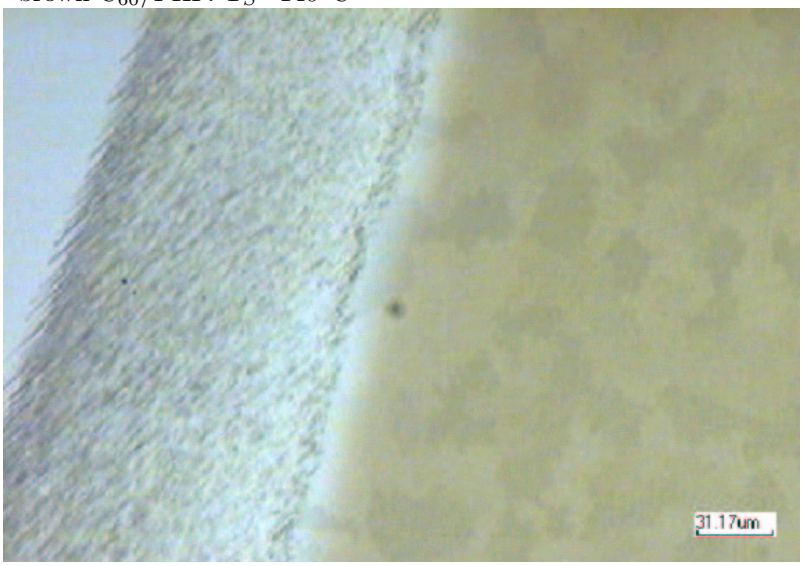

FIGURE 4.6. Sample mcp07: Light microscope picture of C_{60}/PHP bilayer on mica in trough-light geometry. Left PHP, brown C_{60}/PHP. T_S=90°C

1.2. AFM-Studies of PHP films.

1.2.1. *AFM-Studies of PHP films on glass.* A series of films were prepared on glass substrates. The half side of the glass substrates was covered with a thin gold layer. The gold layer is transparent in the visible range. A further advantage is, that you can compare directly the morphology of the films on glass and gold coated glass. Table.4.6 shows the growth conditions of the given AFM pictures.
On amorphous substrates as glass and gold coated glass, no large scale ordered structure can be seen. The growth process starts with the formation of islands. This means, that the growing of the second layer begins before the first is closed. Between the Samples ag01/gl01 and ag02/gl02 the only changed parameter was T_S. At low T_S or not heated substrates, the islands are smaller and the dendritic character is less pronounced due to the smaller "mobility" of the molecules. Compare Fig.4.8, 4.12 and 4.13. Higher T_S enhances the formation of islands resulting in an open film. Sample gl03 was grown without pre- and heating of the substrate during the film growth. Resulting in a very smooth closed film. The film on ITO was grown with the same conditions as sample gl03. Comparison of sample gl03 (fig.4.13) and ito03 (fig.4.15) shows, that the roughness of the PHP film on ITO is at least two times higher. PHP on ITO is forming layered islands with a step-size of around 3-6 nm (see fig.4.16 height profile).

X-ray studies [**43**] and luminescence measurements show, that at higher T_S the molecules are staying perpendicular to the substrate. Too high substrate temperature stops the film growth process completely (sample gl04).

TABLE 4.6. Growth parameter of PHP films

Sample-Nr.	Substrate-material	T_S [°C]	$T_{Wall/Source}$ [°C]	Growth time [min]	Preheat [°C]	Ref Fig.
gl01	glass	90	240	20	90	4.7,4.8
ag01	gold	90	240	20	90	4.7,4.9
gl02	glass	120	240	20	120	4.10,4.12
ag02	gold	120	240	20	120	4.10,4.11
gl03	glass	20-80[2]	240	60	-	4.14,4.13
ito03	ITO	20-80[3]	240	60	-	4.15,4.16
gl04 [4]	glass	180	240	60	-	-

[2] T_S not controlled, heating of the substrate through thermal radiation
[3] T_S not controlled, heating of the substrate through thermal radiation
[4] No film on the substrate

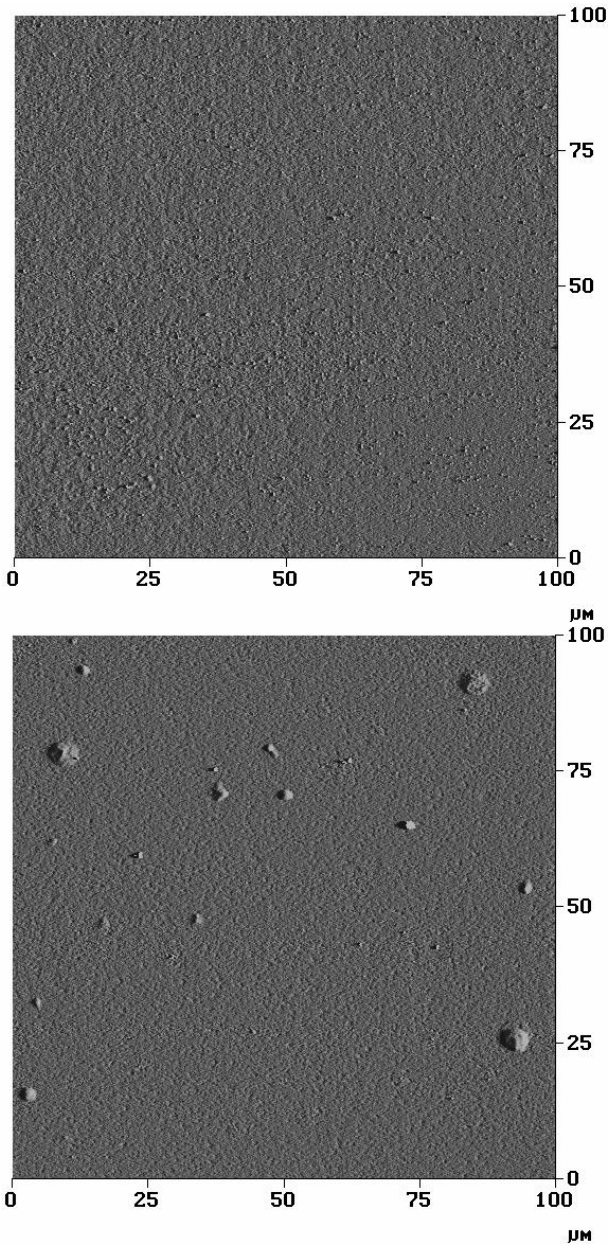

FIGURE 4.7. top: Sample gl01, AFM micrograph of PHP on glass; bottom: Sample ag01, AFM micrograph of PHP on gold. T_S=90°C for both cases.

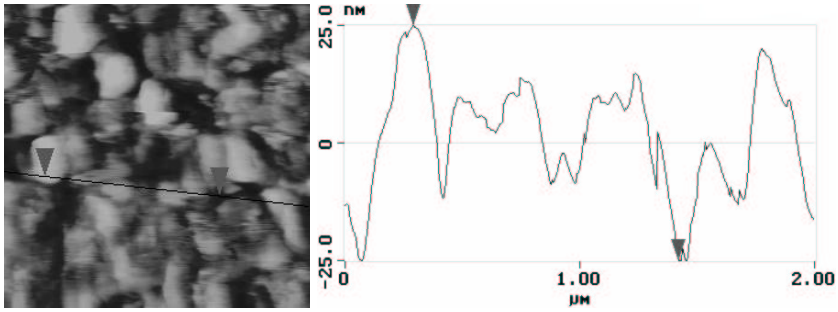

FIGURE 4.8. Sample gl01, AFM section analysis PHP on glass, height between marks $\Delta h = 50$nm. T_S=90°C

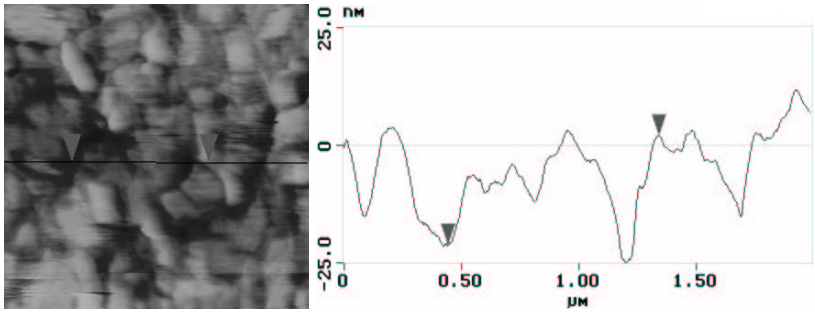

FIGURE 4.9. Sample ag01, AFM section analysis PHP on gold, height between marks $\Delta h = 23$nm. T_S=90°C

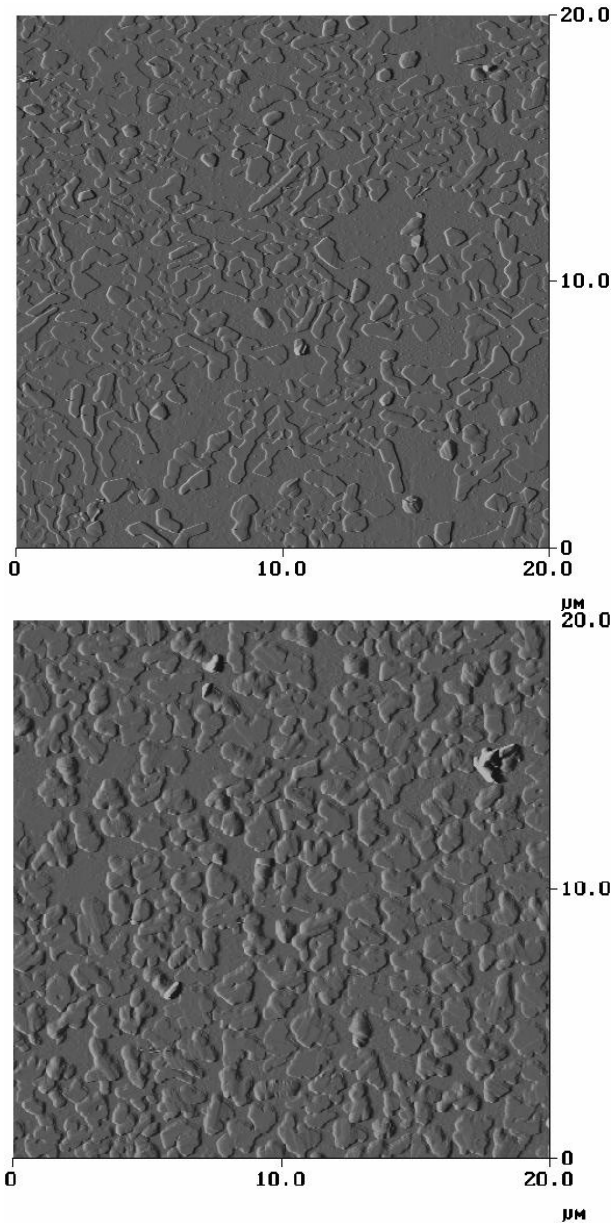

FIGURE 4.10. top: Sample gl02, AFM micrograph of PHP on glass, bottom: Sample ag02, AFM micrograph of PHP on gold coated glass. T_S=120°C for both cases.

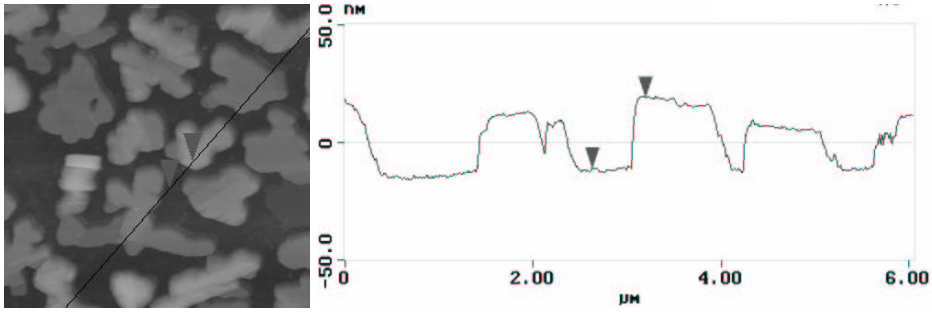

FIGURE 4.11. Sample ag02, AFM section analysis PHP on gold coated glass, height between marks $\Delta h = 23$nm. T_S=120°C

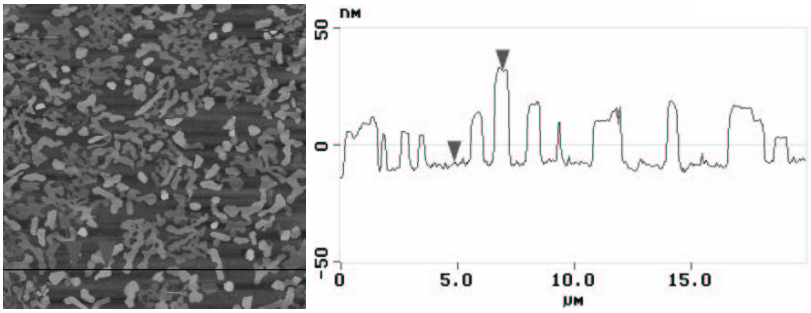

FIGURE 4.12. Sample gl02, AFM section analysis of PHP on glass, height between marks $\Delta h = 39$nm. T_S=120°C

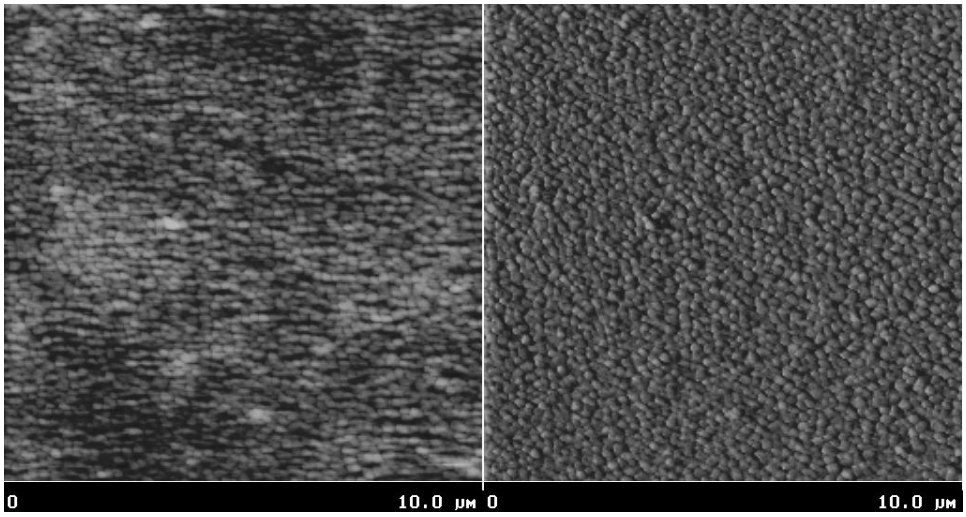

FIGURE 4.13. Sample gl03, left: AFM height profile, Z-range=20nm. Right: micrograph of PHP on glass. T_S=20-80°C

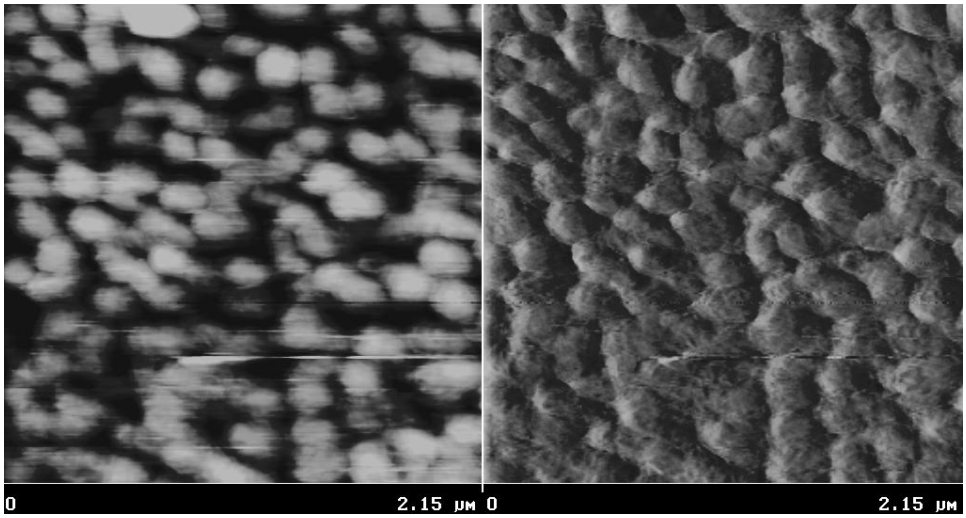

FIGURE 4.14. Sample gl03, left: AFM height profile, Z-range=10nm. Right: micrograph of PHP on glass. T_S=20-80°C

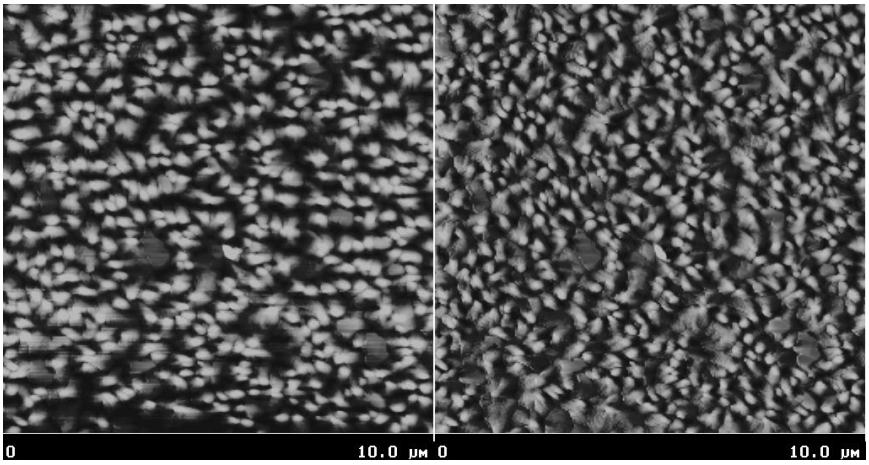

FIGURE 4.15. Sample ito03, left: AFM height profile, Z-range=20nm. Right: micrograph of PHP on glass. T_S=20-80°C

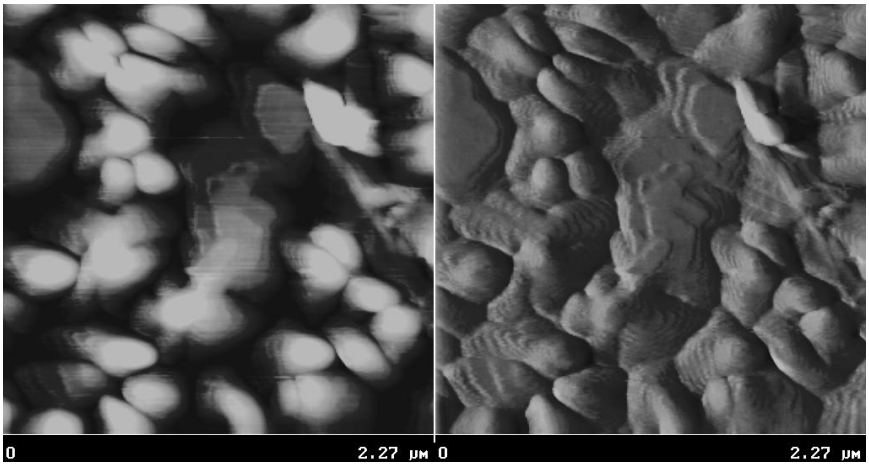

FIGURE 4.16. Sample ito03, left: AFM height profile, Z-range=20nm. Right: micrograph of PHP on glass. T_S=20-80°C

1.2.2. *AFM Studies of PHP on mica.* It has been shown that layered substrate and especially mica, are promising candidates for the epitaxy of thin C_{60} films of high crystalline quality [**40**]. Essentially for the growth process is the lattice confinement. The mismatch of the evaporated material and the substrate lattice-constant should be in the range of percent. In the case of C_{60} on mica it is 3.4 percent [**1**]. PHP also "fits". The distance between the phenyl rings is 5.12 A and the mica lattice constant is 5.2 Å resulting in a lattice mismatch of 1.5 percent. The luminescence plotted as function of the excitation wavelength (action spectrum) of PHP on mica (see fig.4.31) indicates that the molecules are arranged mainly parallel to the substrate.

Table 4.16 shows the sample growth parameters of the given AFM pictures. As on glass, higher T_S enhances the forming of large oriented structures. These structures look like "needles". These needles can be several hundred μm long have a height of ∼50 nm and are several hundred nm wide (sample m01). Changing T_S from 90°C to 140°C the needles become wider (range of μm) an higher ∼250nm. In both cases PHP is homogeneously distributed all over the substrate and the PHP films are not closed. See height profile in fig.4.22,4.23. The films were stable on air but very soft and the AFM-tip made damages on the film surface. Fig.4.20 was taken after fig. 4.19. It clearly shows the area of the scan of fig. 4.19 in fig. 4.20 observable.

TABLE 4.16. Growth parameter of the PHP films on mica

Sample-Nr.	T_S [°C]	T_{Wall} [°C]	T_{Source} [°C]	Growth time [min]	Preheat [C°]	Ref Fig.
m01	90	240	240	20	90	4.17,4.18,4.22
m02	140	240	240	20	140	4.19,4.20,4.21,4.23,4.24

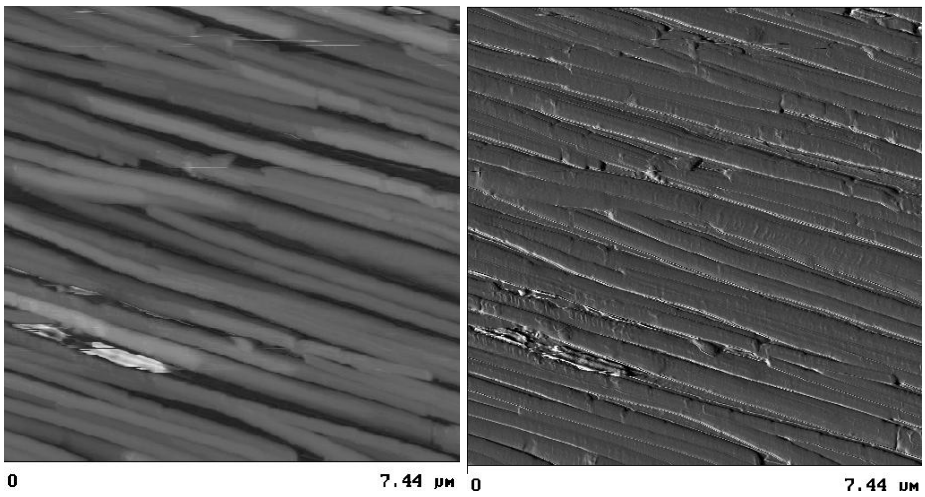

FIGURE 4.17. Sample m01: PHP on mica. Left height-profile, right micrograph. T_S=90°C

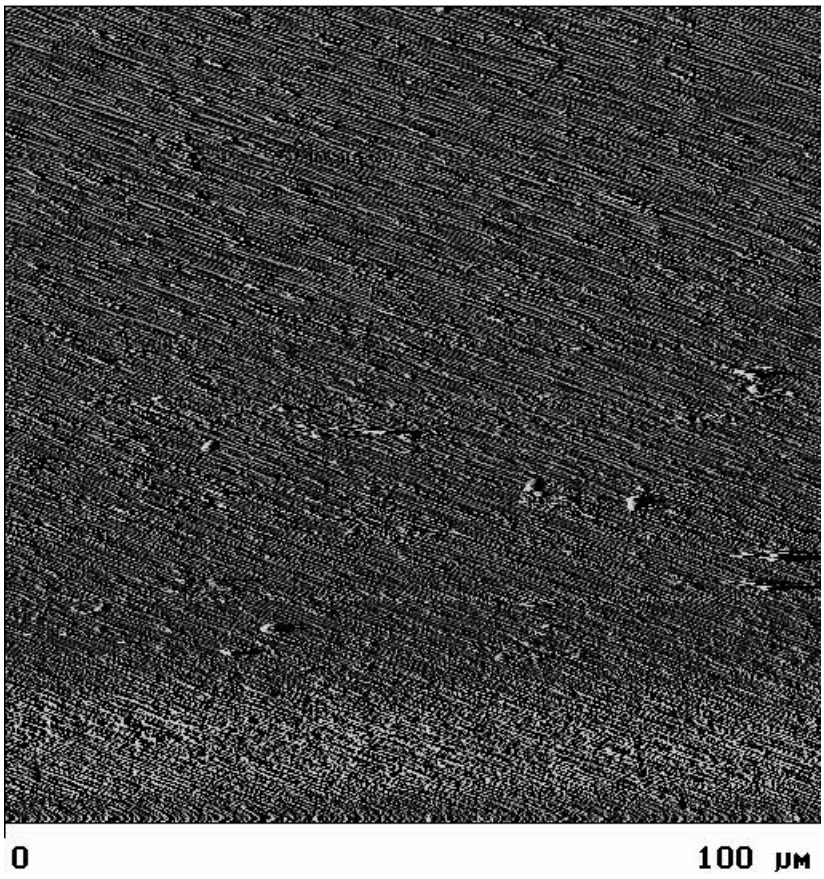

FIGURE 4.18. Sample m01, micrograph of PHP on mica T_S=90°C.

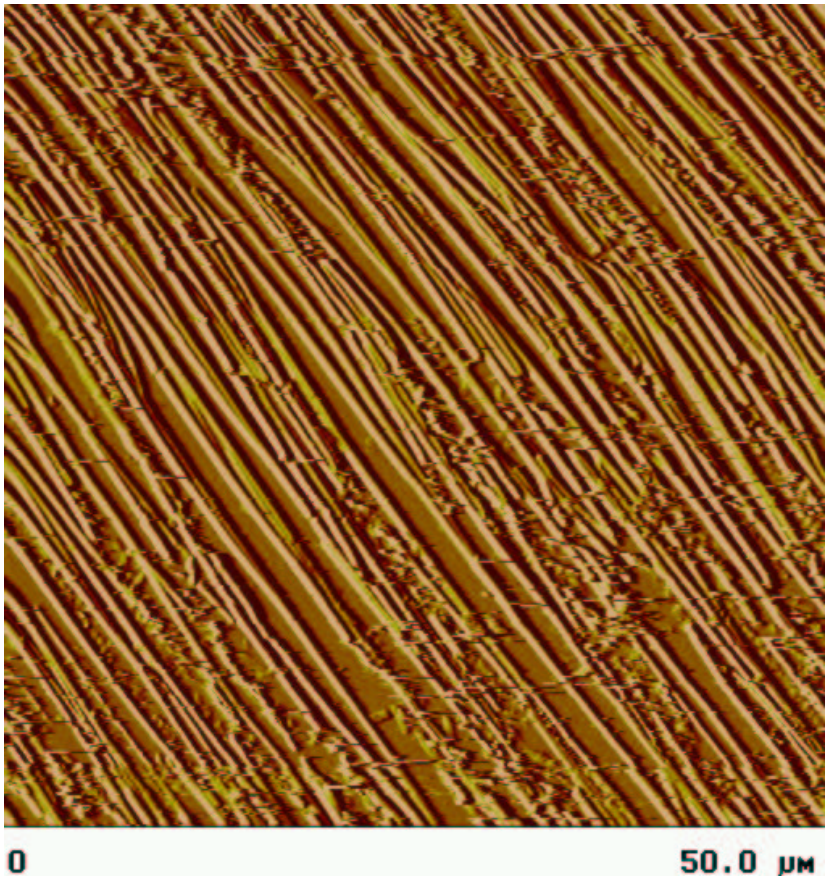

FIGURE 4.19. Sample m02: micrograph of PHP on mica. T_S=140°C

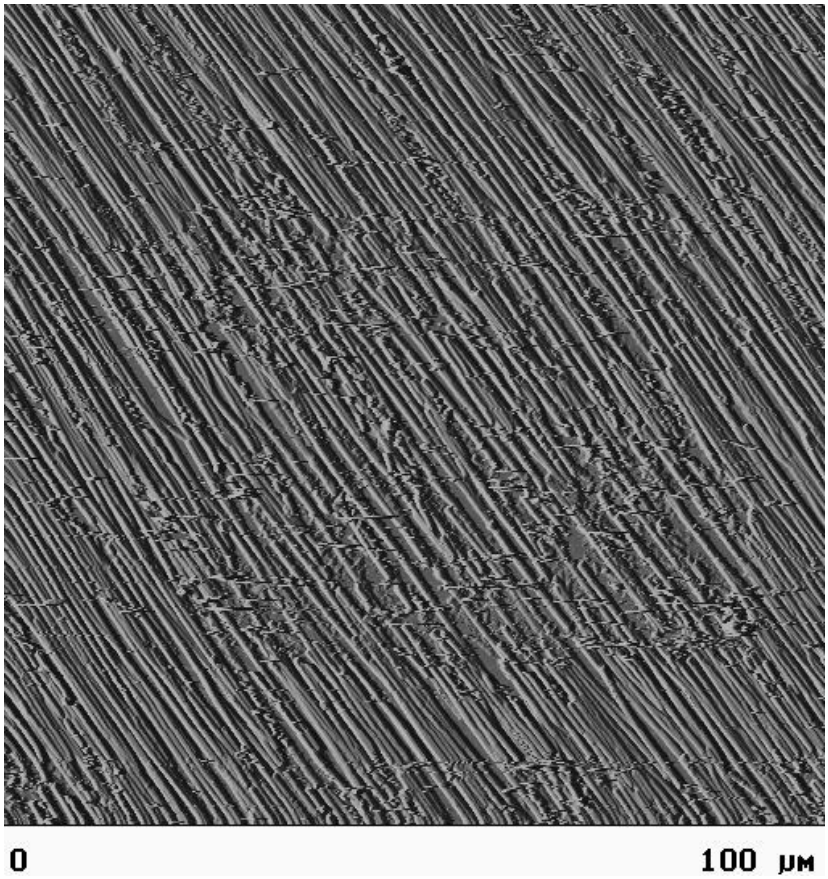

FIGURE 4.20. Sample m02: micrograph of PHP on mica. T_S=140°C

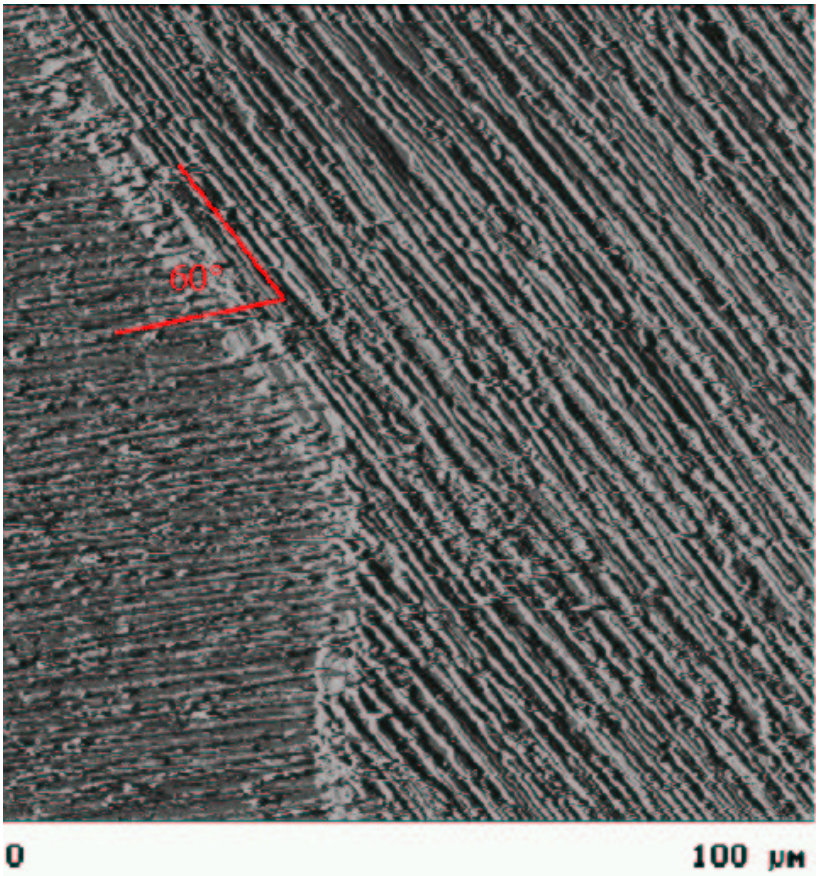

FIGURE 4.21. Sample m02: micrograph of PHP on mica. T_S=140°C

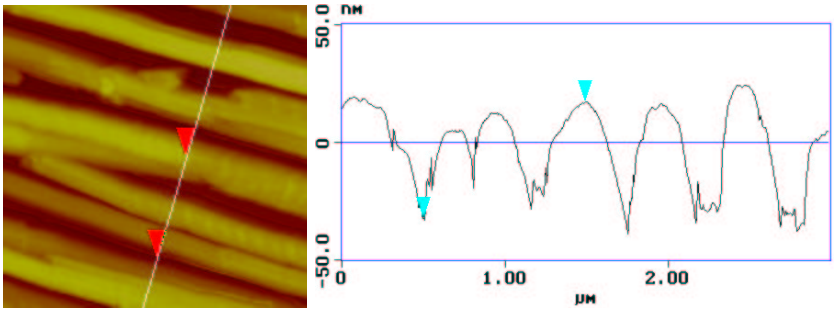

FIGURE 4.22. Sample m01: AFM section analysis PHP on mica, T_S=90°C; height between marks $\Delta h = 49nm$

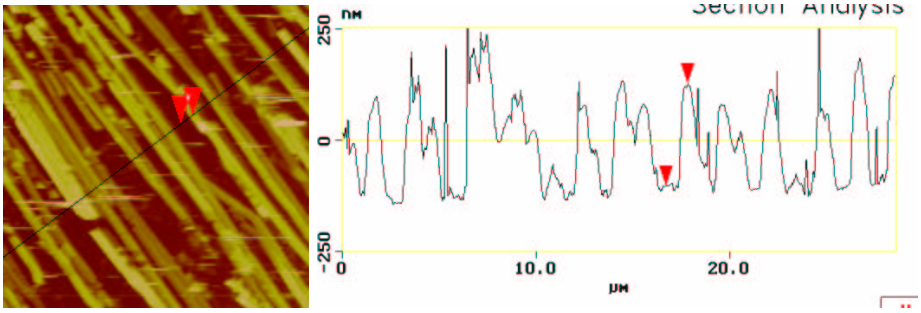

FIGURE 4.23. Sample m02: AFM section analysis of PHP on mica, T_S=140°C; height between marks $\Delta h = 230nm$

In fig.4.21 a change of the direction of the "needles" was found, the angle between the PHP needles are 120° or 60° respectively, in agreement with the threefold symmetry of the cleaved mica surface. The growth process was distort by a step on the mica surface (see section analysis in fig. 4.24). On perfect cleaved mica the orientation of the needles does not change.

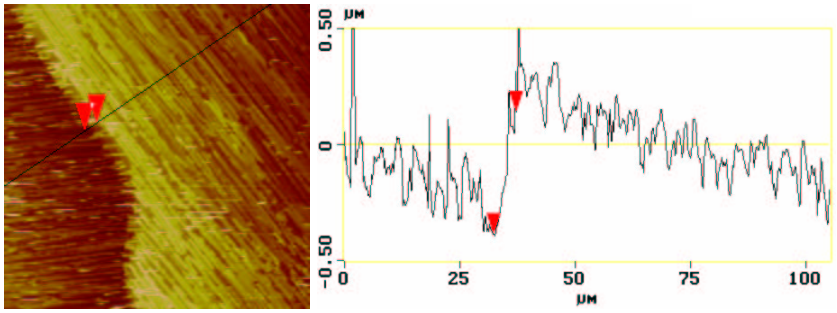

FIGURE 4.24. Sample m02: AFM section analysis PHP on mica, T_S=140°C; height between marks $\Delta h = 530nm$

Such highly oriented films are interesting subjects for further work. The morphology of the needles is not clear. X-ray studies are required and non-linear optic behaviors are expected.

1.3. AFM studies of PHP/C_{60} bilayer on mica. The unique setup in HWE with two sources allows the production of bi- and multilayers, just by changing the position of the substrate from one oven to the another. It has been shown that layered crystals, like MoS_2 and mica, are promising substrate materials for epitaxial growth of C_{60} . Especially for [001] oriented mica, the existence of well aligned [111]-C_{60} planes parallel to the surface was proven. In our work for the preparation of the C_{60} films, the optimized parameter given in [**2**] were used. Resulting in perfect mono-crystalline C_{60} films. On such films we studied the growth process of PHP.

The only changed parameter was T_S. As on glass and mica, higher T_S enhances the forming of oriented islands.

TABLE 4.24. Growth parameter of PHP/C_{60} bilayer on mica

Sample-Nr.	T_S [°C]	PHP T_{Wall}= T_{Source} [°C]	C_{60} T_{Wall}= T_{Source} [°C]	PHP/C_{60} Growth time [min]	Preheat [°C]	Ref Fig.
mcp01	90	240	400	20/20	90	4.25,4.26
mcp02	120	240	400	20/20	120	4.27,4.29
mcp03	140	240	400	20/20	140	4.28,4.30

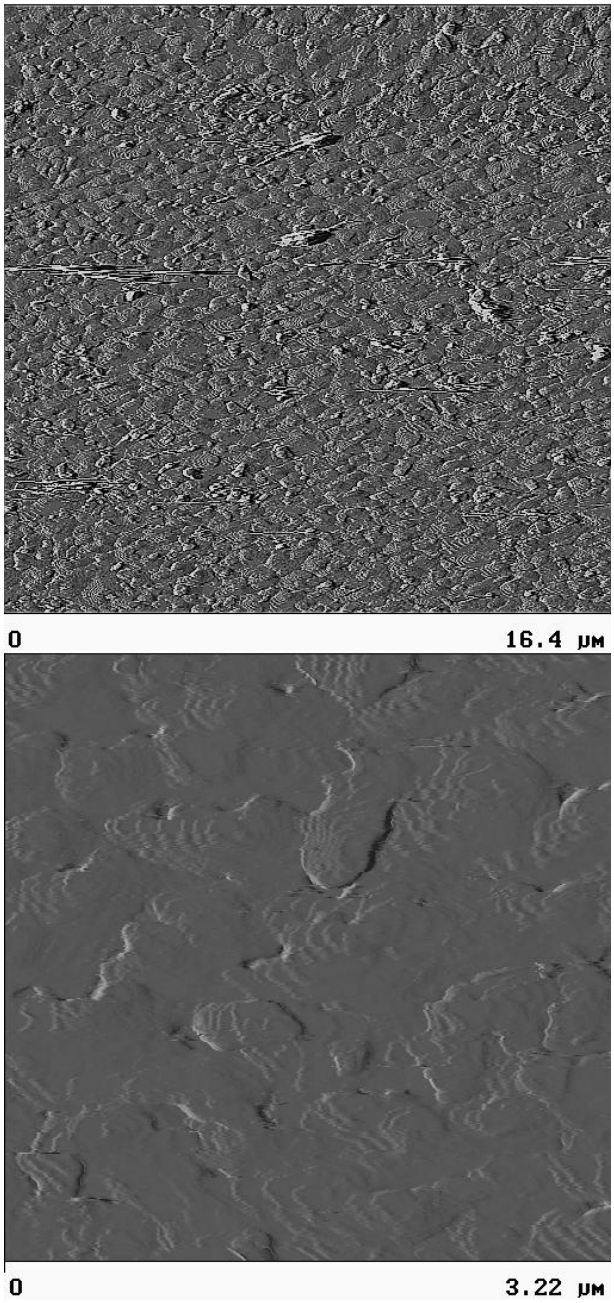

FIGURE 4.25. Sample mcp01: AFM micrograph of PHP on C_{60} coated mica; T_S=90°C

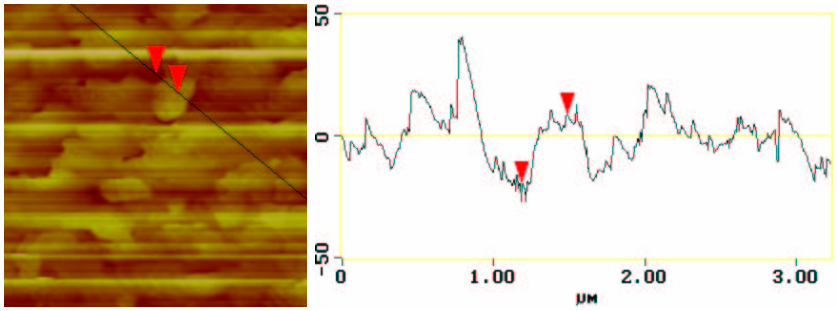

FIGURE 4.26. Sample mcp01: AFM section analysis PHP on C_{60} coated mica; T_S=90°C; height between marks $\Delta h = 28nm$

On sample mcp01 and mcp02 (fig 4.25,4.27) we can identify layered islands. This indicates the growth of separated PHP layers resulting in a homogeneously covered film. Such a growth is called quasi-epitaxial growing. If the mobility of the PHP molecules is high enough, they are forming structures following the symmetry of the C_{60} surface see fig. 4.28. The angle between the islands is again 60°/120° or 90° respectively. C_{60} molecules on mica are forming FCC (face-centered) film surfaces this results in a sixfold symmetry parallel to the substrate.

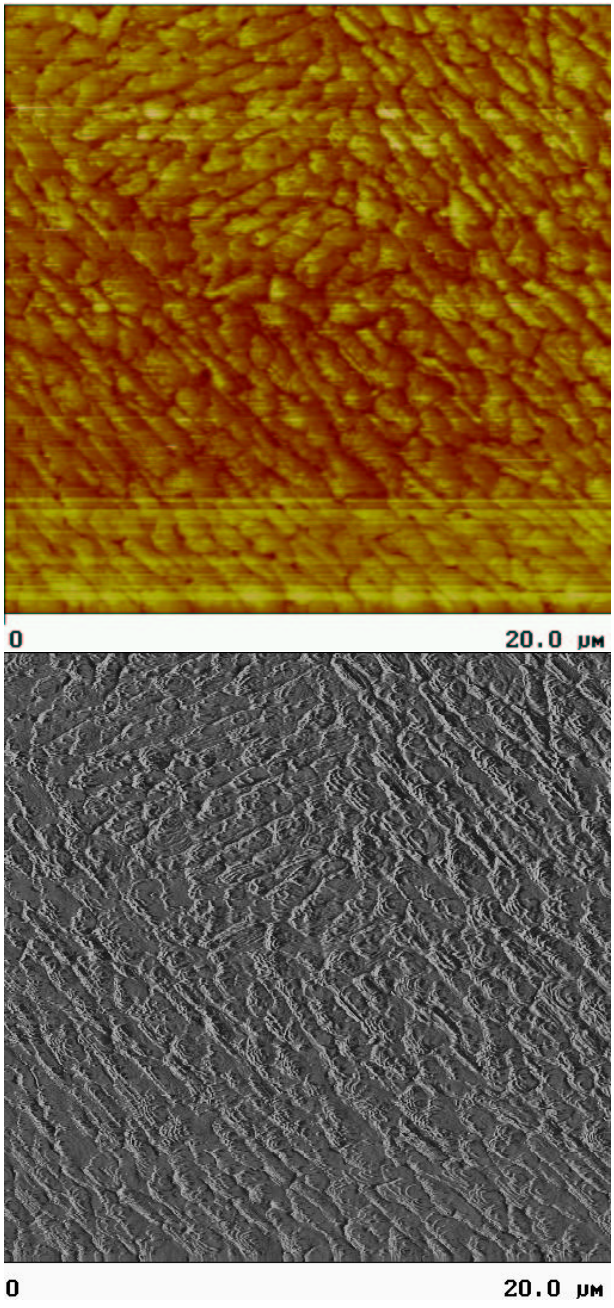

FIGURE 4.27. Sample mcp02: top: height profile of PHP on C_{60} coated mica; bottom: micrograph of PHP on C_{60} coated mica. T_S=120°C

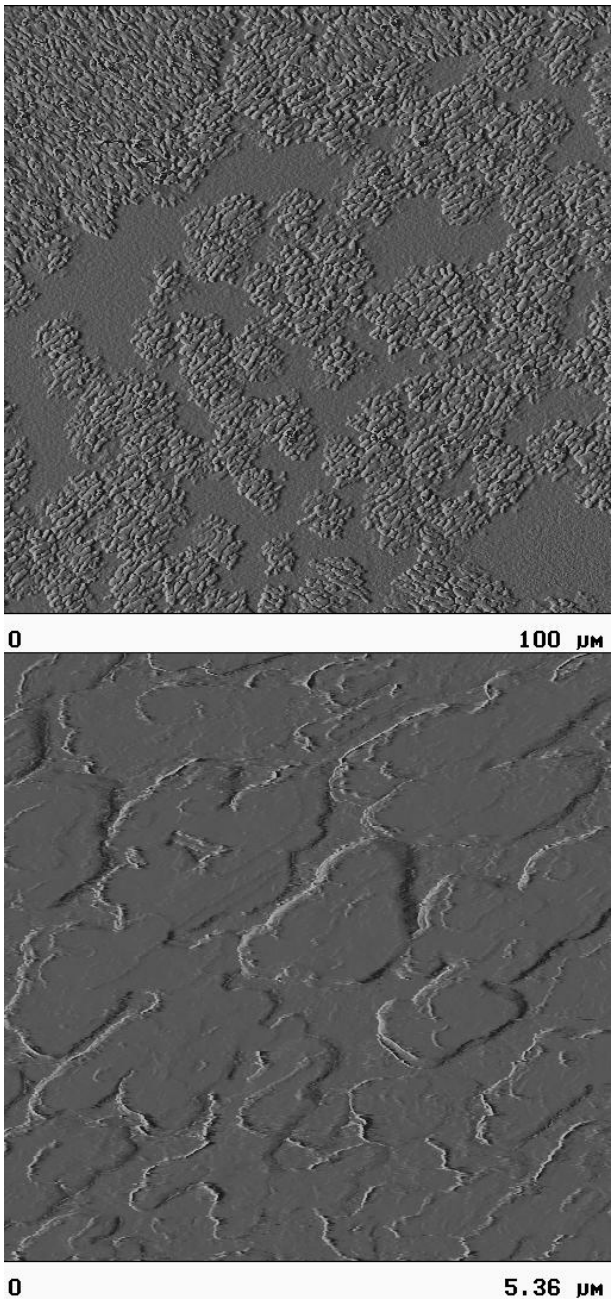

FIGURE 4.28. Sample mcp03: AFM micrograph of PHP on C_{60} coated mica; T_S=140°C

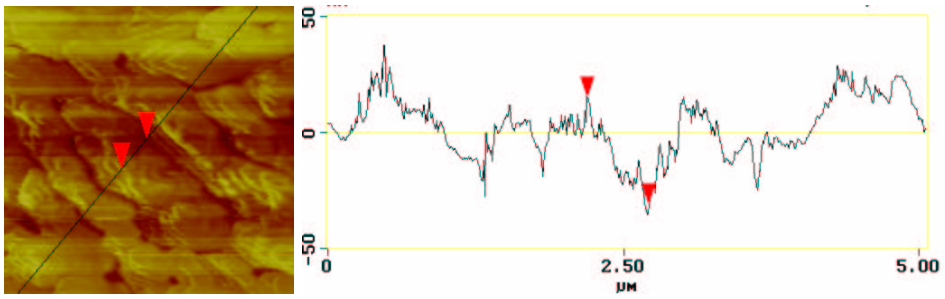

FIGURE 4.29. Sample mcp02: AFM section analysis PHP on C_{60} coated mica; T_S=120°C; height between marks $\Delta h = 46nm$

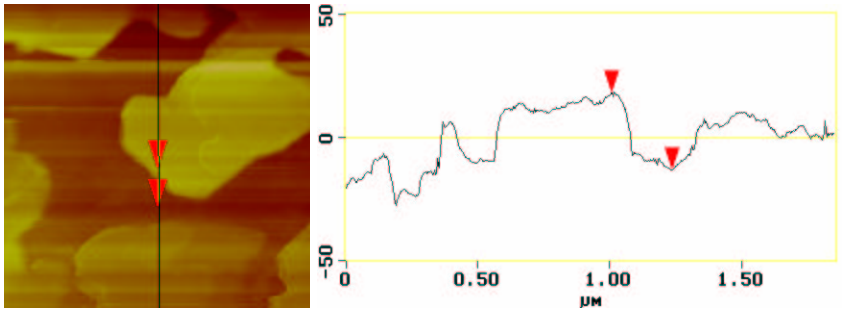

FIGURE 4.30. AFM section analysis PHP on C_{60} coated mica; T_S=140°C; height between marks $\Delta h = 31nm$

At high T_S= 140°C the PHP film is not closed and the islands become a very flat top (fig.4.30). This is a good starting point for further work. Variation of the deposition rate and the growth time are required.

2. Photoluminescence studies on thin PHP-films

In this chapter detailed photoluminescence studies of thin PHP-films on different substrates are shown. Efficient excitation of luminescence is observed for excitation energies above 3.1 eV (400nm). The peak position of the PL excitation spectrum is determined by a superposition of the absorption parallel and perpendicular to the backbone. Theoretical calculations using linearized augmented plane wave (LAPW) method [**3**] predict a strong anisotropy between the dielectric coefficients parallel and perpendicular to the chain. For excitation perpendicular to the chain the absorption starts around 410 nm (90°) and is blue shifted for smaller angles between excitation-light and the chain-orientation. See fig. 4.31.

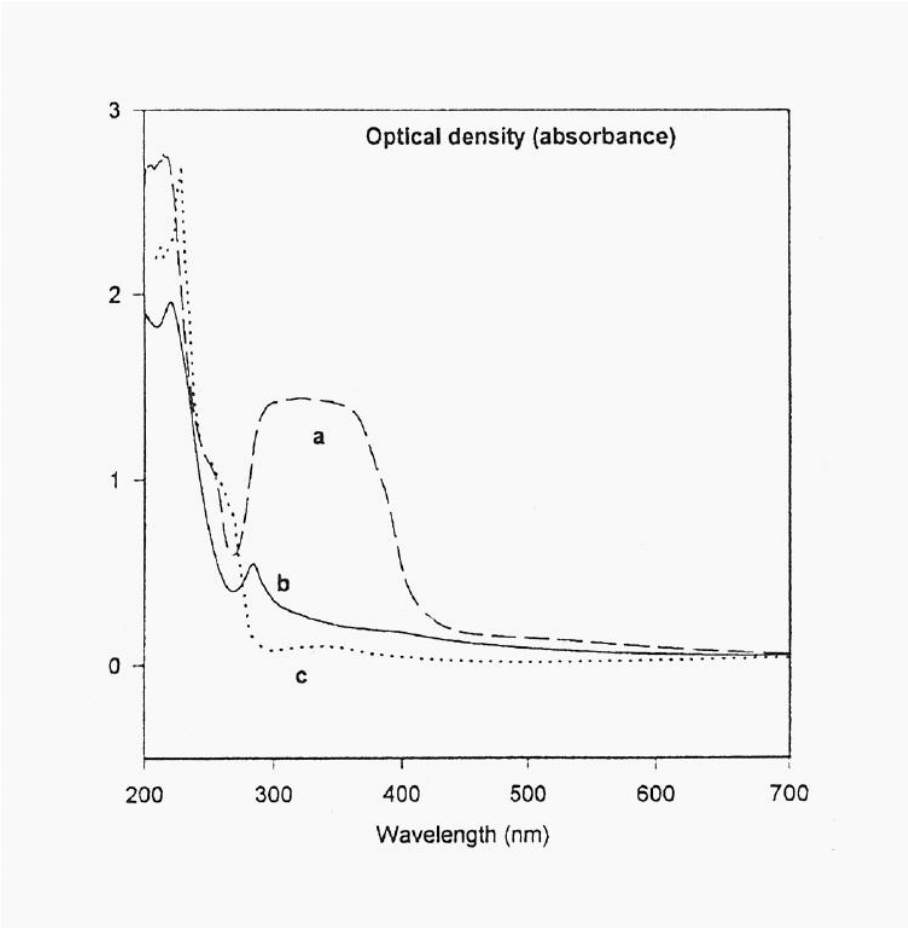

FIGURE 4.31. left: Variation of optical absorption with PHP orientation. right: Measured and calculated optical density for PHP: (a) polycrystalline film (experiment], (b) oriented film (experiment); (c) oriented film (theory). Taken from ref. [**3**].

Action spectra of PHP on mica and ITO are given. The excitation beam illuminated the film perpendicular ($\alpha = 0°$) and parallel to the substrate ($\alpha = 90°$). The excitation-spectrum on ITO (fig.4.32 and 4.33) indicates molecules are staying perpendicular to the substrate. In contrast, on mica the chains are arranged mainly parallel to the substrate fig.4.34.

TABLE 4.31. Growth parameter of PHP films

Sample-Nr.	Substrate-material	T_S [°C]	$T_{Wall/Source}$ [°C]	Growth time [min]	Preheat [°C]	Ref Fig.
gl02	glass	90	240	30	90	4.36
ito03	ITO	140	240	30	140	4.36,4.32,4.33
mic03	mica	90	240	10	90	4.36,4.34,4.37

The different action-spectrum on mica and ITO can be understood by comparison with the calculated spectra. The vertical transitions in the k-space are symmetry allowed if the excitation beam acts parallel to the molecular chain and the vertical transitions are symmetry forbidden if the excitation beam excite the molecule perpendicular to the chain.

TABLE 4.31. Calculated and measured optical transmissions of thin PHP films

transmission	E_{theory} [eV]	λ_{theory} [nm]	$\lambda_{measured}$ on ITO [nm]	$\lambda_{measured}$ on mica [nm]
0-0	3.08	402	410	-
0-1	3.72	332	330	330
0-2	4.66	266	-[5]	-
1-1	4.37	280	283	-

On the ITO sample (ito03) the vertical transitions (fig.4.32) HOMO-LUMO, HOMO-1 - LUMO+1 denoted as 0-0,1-1 and 2-2 and the no- vertical transition (fig.4.33) HOMO - LUMO+1 (0-1) are in agreement with the calculated spectra in tab.4.31.

[5]not measured, but local-minimum in fig.4.32

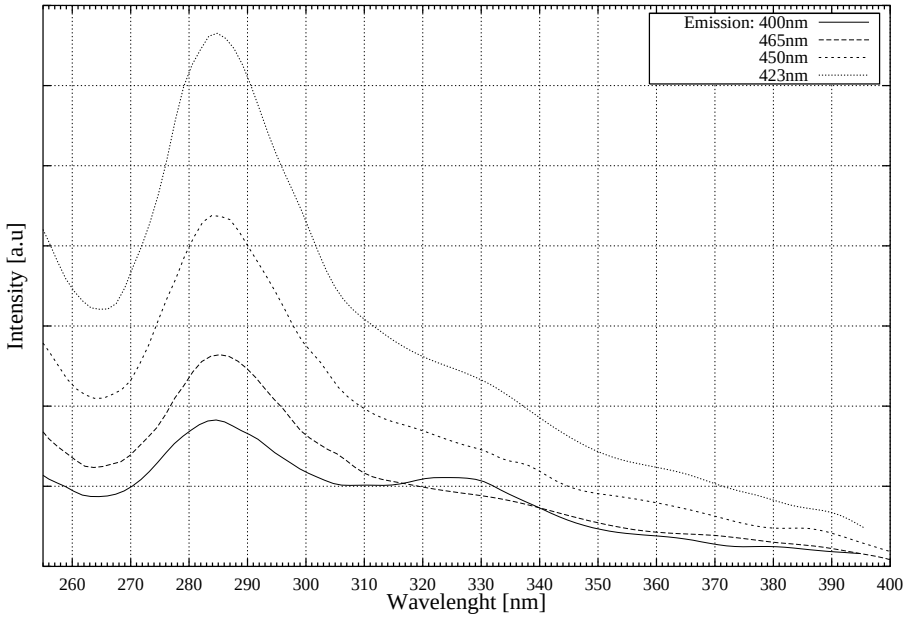

FIGURE 4.32. Sample: ito03; Excitation-spectrum of PHP on ITO. $\alpha = 0°$

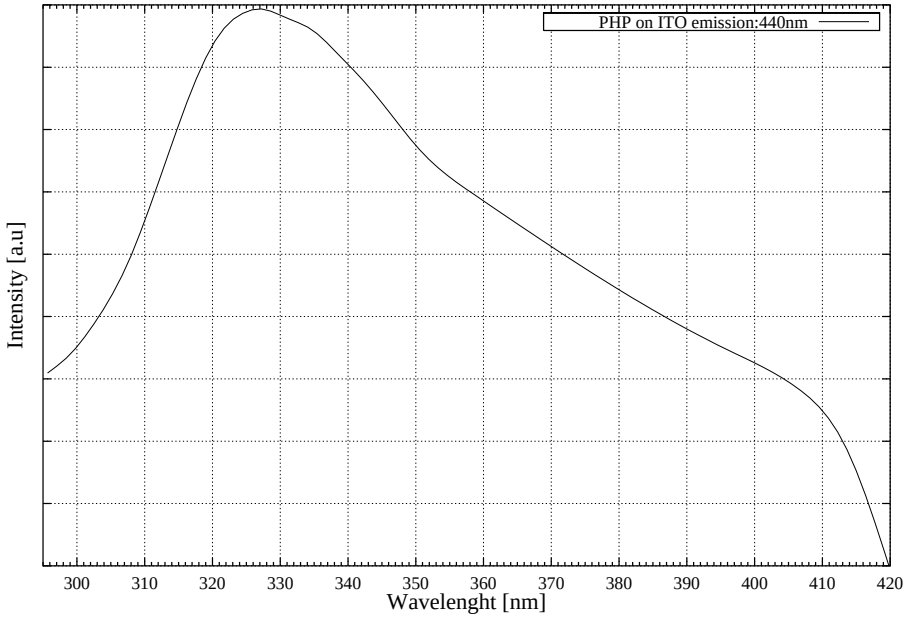

FIGURE 4.33. Sample: ito03; Excitation-spectrum of PHP on ITO. $\alpha = 90°$

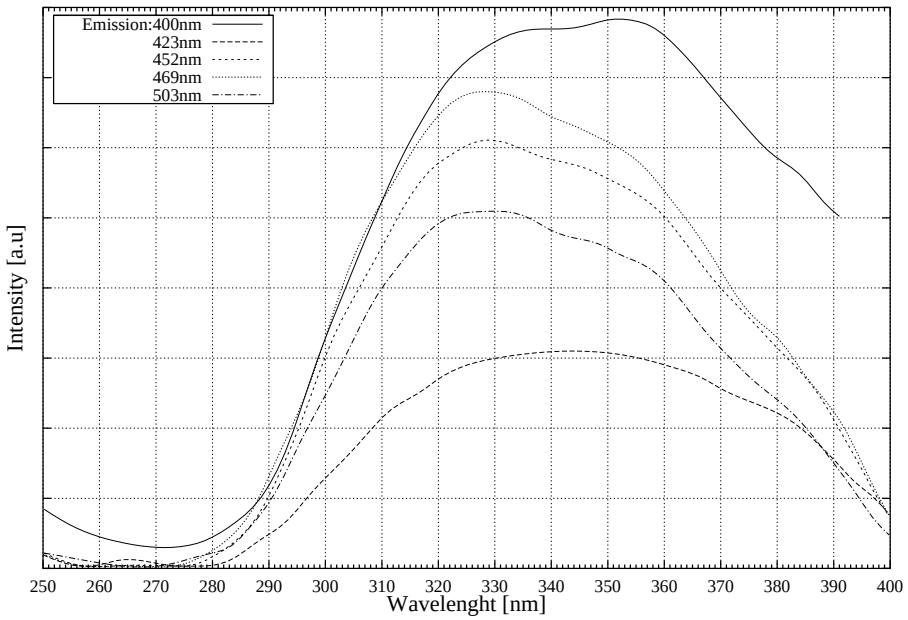

FIGURE 4.34. Sample: mic03; Excitation-spectrum of PHP on mica. $\alpha = 0^\circ$

Non vertical transitions in k-space are induced by excitation perpendicular to the chain (fig.4.33),4.34). Due to the finite size of the PHP-molecule the k-vector of the wavefunction is not longer a good quantum-number and non-vertical transitions with a small induced k vector are possible.[6] The broad signal of the action-spectrum on mica and ITO by excitation perpendicular to the chain cannot bee understood by applying the simple band-structure model and seems to be a intermolecular effect. One explanation is the so called Davydov-splitting interaction (fig.4.35). When two adjacent oligomers are aligned along the same axis, The exited state will split into exciton levels by Davydov interaction. The transition dominant dipole are aligned along the chain. The magnitudes of the dipole strengths connection the ground state with these two exciton levels is determined by the intrinsic dipole strength of the oligomers and their relative orientation: $D^{\pm} = (1/2)(\vec{\mu}_{a0n} \pm \vec{\mu}_{b0n})^2$, where $\vec{\mu_{0n}}$ is the electric transition moment of the $|0\rangle \rightarrow |n\rangle$ transition. It is important to not that when two identical transition dipole moments are exactly parallel, excitation to (and emission from) the lowest level is formally forbidden and no (or a small) splitting occurs [**44**]. The magnitude of the Davydov splitting depends on the intermolecular distance. The relationship between optical properties of oligothiophenes and their microcrystalline structure has been investigated by Garnier et al [**45, 46, 47**]. In thin 6T polycrystalline films a wide excitonic band was interpreted as the lower level of the Davydov splitting.

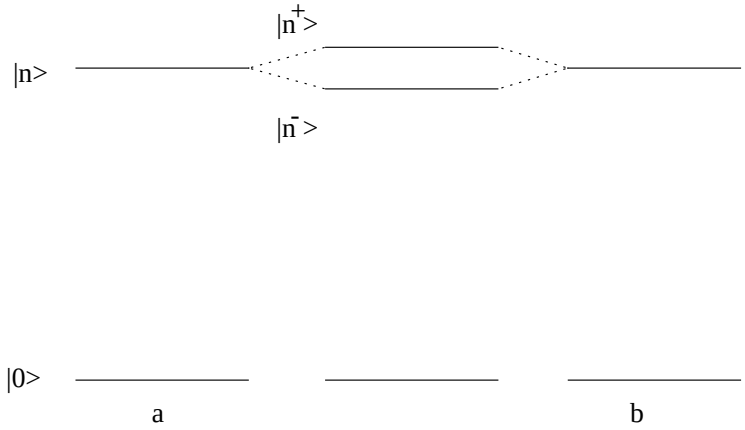

FIGURE 4.35. Schematic energy diagram of exciton (Davydov) splitting

The PL emission spectra shows vibrational fine-structure, mainly determined by the C=C stretching of the backbone [**48**]. The presence of vibrational structure indicates a strong electron-phonon coupling. In [**44**] it was shown that the photoluminescence spectrum of oligothiopenes is invariant to the excitation wavelength as long as it lies within the $\pi - \pi^{\star}$ absorptions band. Such vibrational fine-structure was also observed in para-quarter-phenyl. The spectra strongly depends on the morphology of the sample. In a common picture the origin of the luminescence is the existence of a long-living state in the band-gap and the broad background is due to emission from defect states, but their density and nature are strongly depend on the film morphology [**49**].

In fig. 4.37 the photoluminescence (PL) emission of PHP on mica at room temperature and helium-temperature are shown. At room-temperature the spectra on mica become a broad signal due longer wavelengths.

[6]No vertical transitions occurs by changing the nuclear geometry

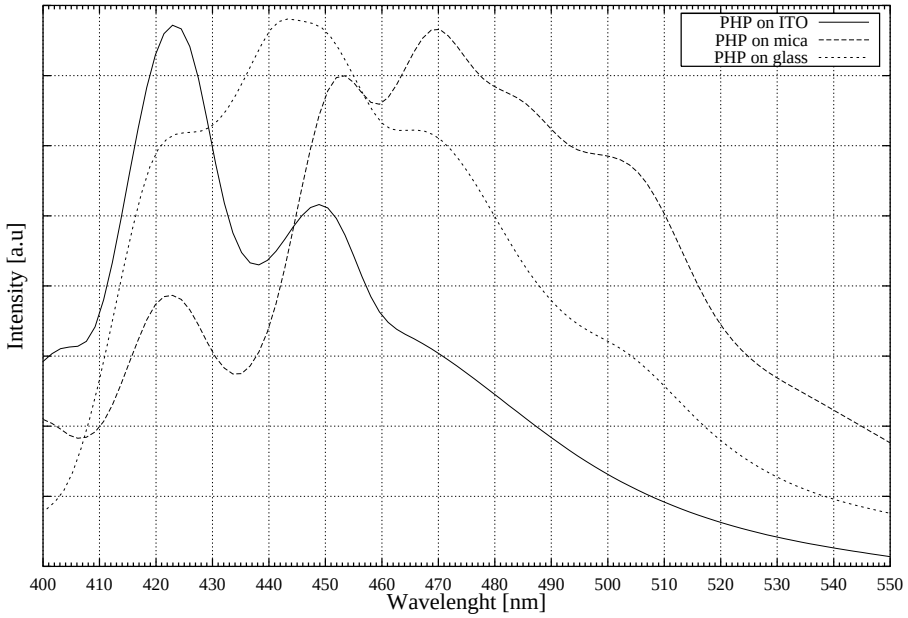

FIGURE 4.36. Normalized luminescence spectra of PHP on mica (mic03), glass (gl02), ITO (ito03). Excitation-wavelength=350 nm

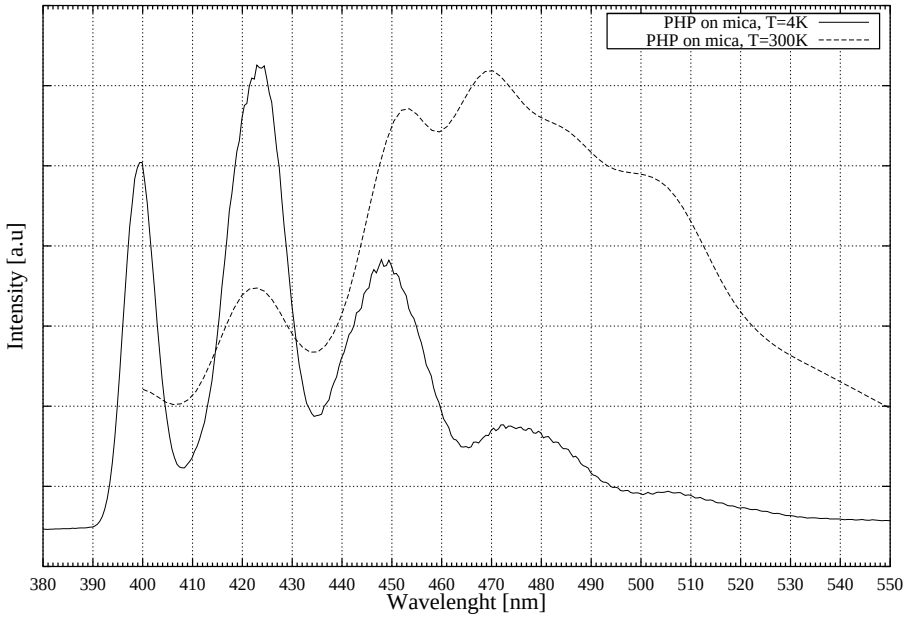

FIGURE 4.37. Sample mic03: Normalized luminescence spectra of PHP on mica at 4K and room-temperature. Excitation-wavelength=350 nm

3. Luminescence studies on PHP and C_{60}/PHP bilayer structures

On cleaved mica substrates PHP films and C_{60}/PHP bi-layer structures with the optimized growing conditions for C_{60}-layer given in [**1**] and a low substrate temperature of T_S= 90° for PHP-layer was chosen. Due to the ultrafast electron-transfer to C_{60} [**13**] a quenching of the photoluminescence is observed. The strong photoluminescence of PHP is quenched by one order of magnitude at 4K (fig.4.38) and become more efficient at higher temperatures (fig.4.40). The quenched photoluminescence spectra of sample mic12 and mic13 shows no shifting to higher or lower energies or new spectral resolved species and indicates no new radiative states below the $\pi - \pi^\star$ gap of PHP. The excitation was provided by the 350.7 nm line of an argon-laser. The C_{60} luminescence occurs above 690nm at low temperature and the shape is in agreement with measurements in [**2**]. These measurements are not finished. The temperature dependent photo-luminescence of pure PHP films and C_{60} /PHP bilayers with different growing conditions are required.

TABLE 4.37. Growth parameter of PHP film and C_{60}/PHP-bilayer on mica

Sample-Nr.	T_S [°C]	$T_{Wall/Source}$ PHP/C_{60} [°C]	Growth time C_{60}/PHP[min]	Preheat [°C]	Ref Fig.
mic11	90	400/240	-/10	90	4.38
mic12	140/90	400/240	30/10	140/90	4.38, 4.39, 4.40
mic13	140/90	400/240	10/10	140/90	4.38

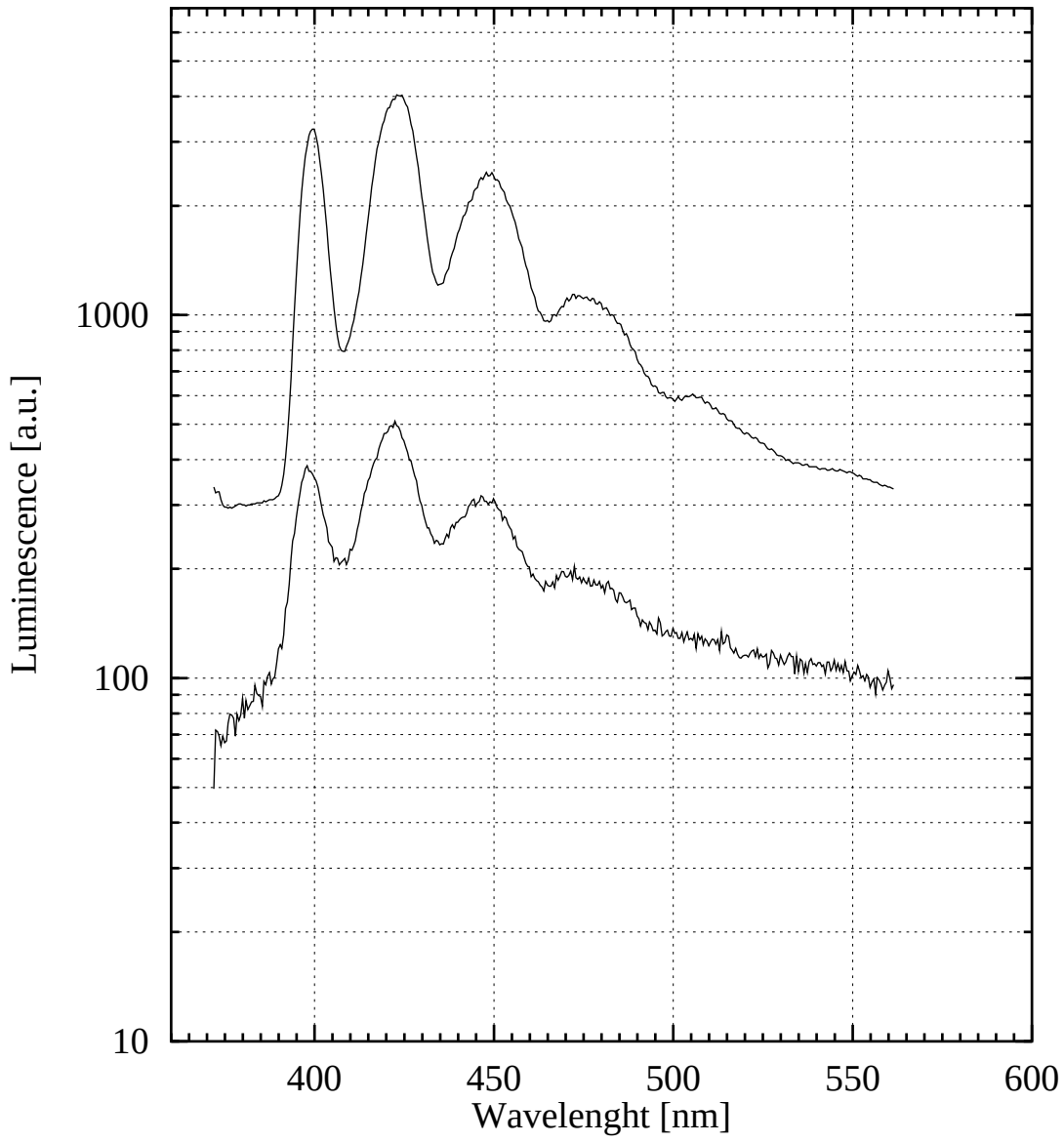

FIGURE 4.38. Sample: mic12; Luminescence of PHP (top curve) and C_{60}/PHP bilayer (bottom curve) at 4K. Thickness PHP: 30nm, C_{60}: 90nm. Excitation-wavelength 350.7 nm

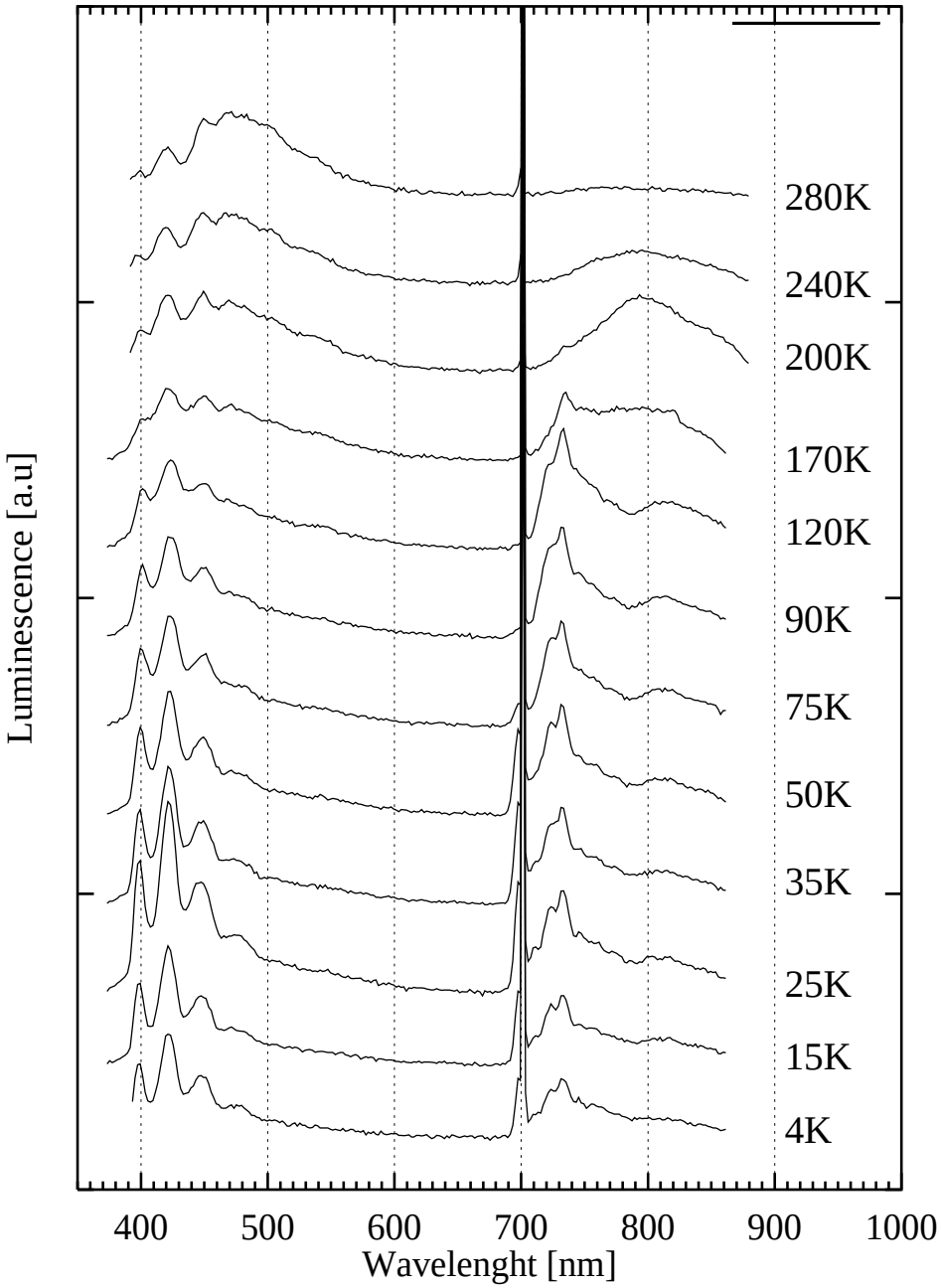

FIGURE 4.39. Temperature depended luminescence of C_{60}/PHP bilayer (sample mic12). Spectra are offset to clarify the presentation. Excitation-wavelength=350.7 nm

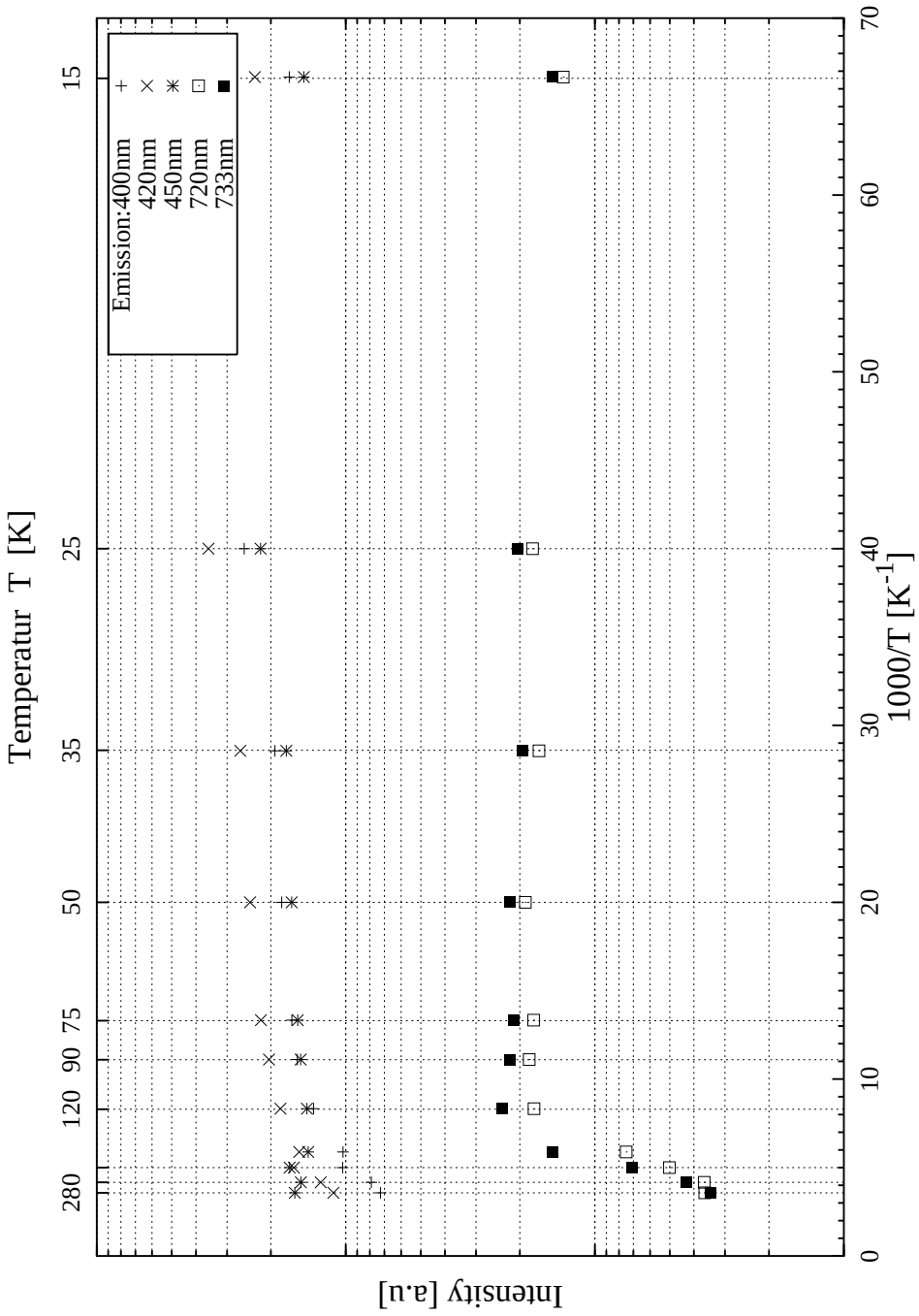

FIGURE 4.40. Arrhenius-plot of the C_{60}/PHP bilayer (sample mic12) luminescence. The PHP emission lines at 400,420 and 450 nm are plotted with the factor of 10 to clarify the presentation. Excitation-wavelength=350.7 nm

4. Polarized photoluminescence

PHP on glass is forming very smooth films. No large ordering was observed. The films are poly-crystalline. However the luminescence shows a strong anisotropic effect. In fig. 4.41 the two used geometries are given. In the excitation beam and in front of the detector polarizers were installed.

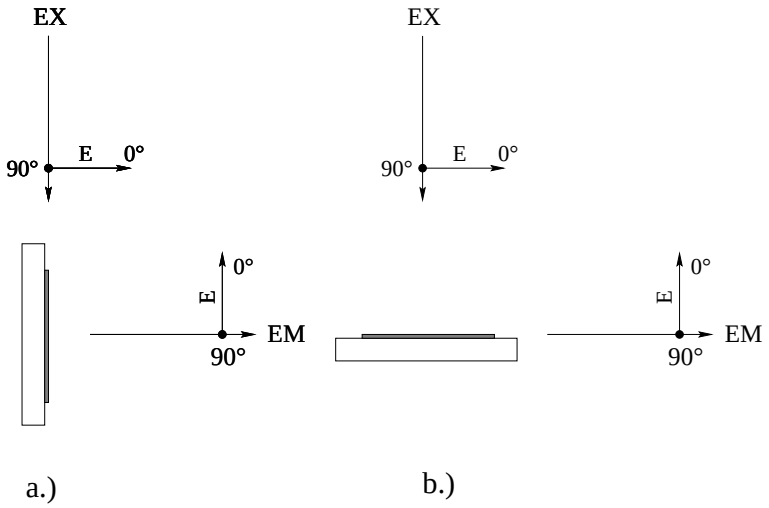

FIGURE 4.41. Geometry of the polarized luminescence setup

In case a) the excitation light illuminated the film parallel to the substrate and in the other case b.) the illumination acts perpendicular to the film surface. Polarization directions are given relative to the plane defined by the incident beam (excitation) and luminescence beam.

4.1. Polarized photoluminescence on PHP-films on glass. A polarization effect of the luminescence was found by changing the polarization of the excitation beam or the illumination beam, if they are acting parallel to the substrate. And no (or a small) polarized effect of the luminescence was found by changing the polarization of the excitation beam or the illumination beam, if they are acting perpendicular to the substrate.

The absorption of PHP [**3**] is anisotropic. High optical densities are expected if the electric field vector acts parallel to the chain of the molecules. This yields in a polarization effect of the excitation beam or luminescence respectively. So we conclude that the molecules are standing perpendicular to the substrate. The excitation wavelength was set to 350nm. These findings are in agreement with X-ray studies of MBE grown PHP films [**43**].

TABLE 4.41. Growth parameter of PHP films

Sample-Nr.	Substrate-material	T_S [C°]	$T_{Wall/Source}$ [C°]	Growth time [min]	Preheat [C°]	Ref Fig.
gl018	glass	140	240	30	140	4.42,4.43

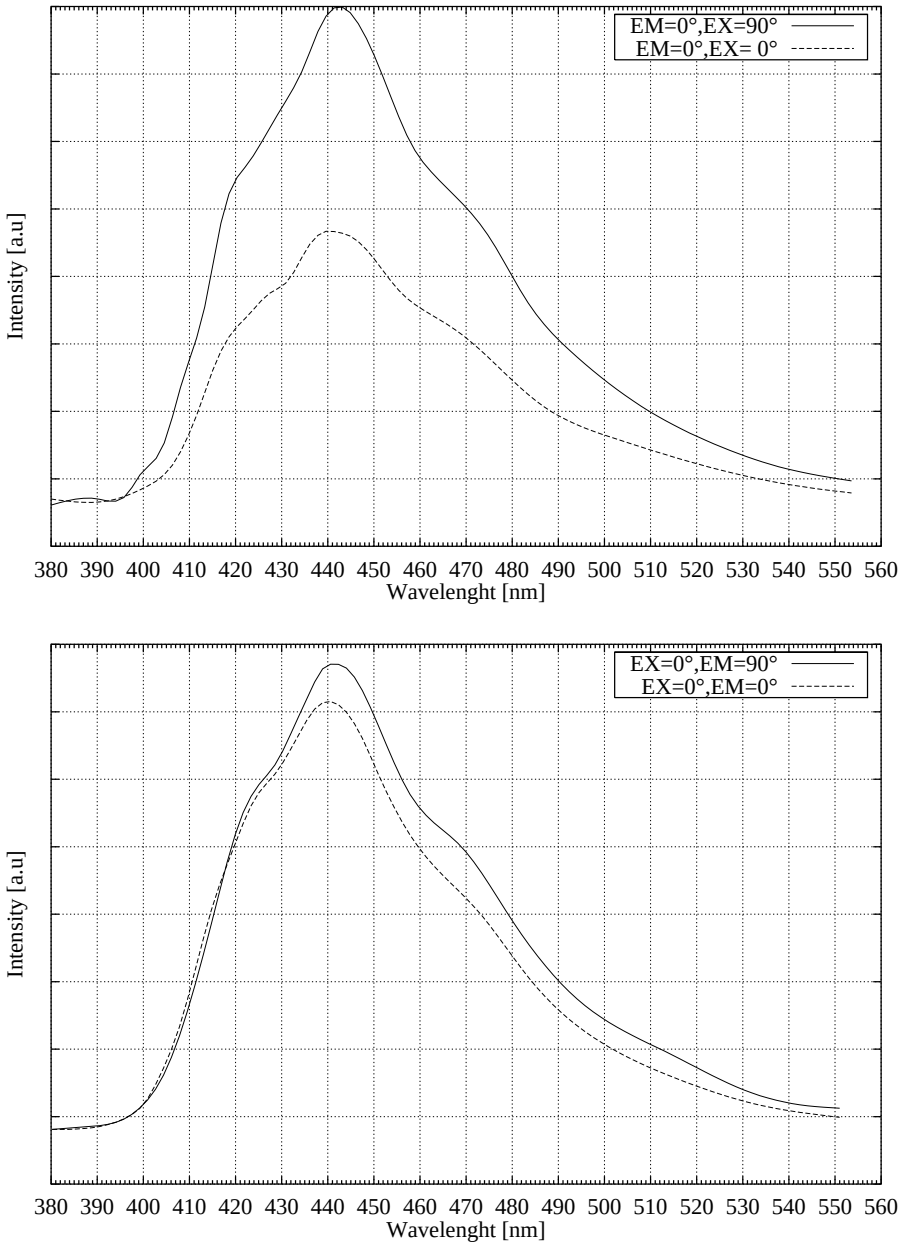

FIGURE 4.42. Sample: gl018; polarized luminescence of PHP in geometry a)

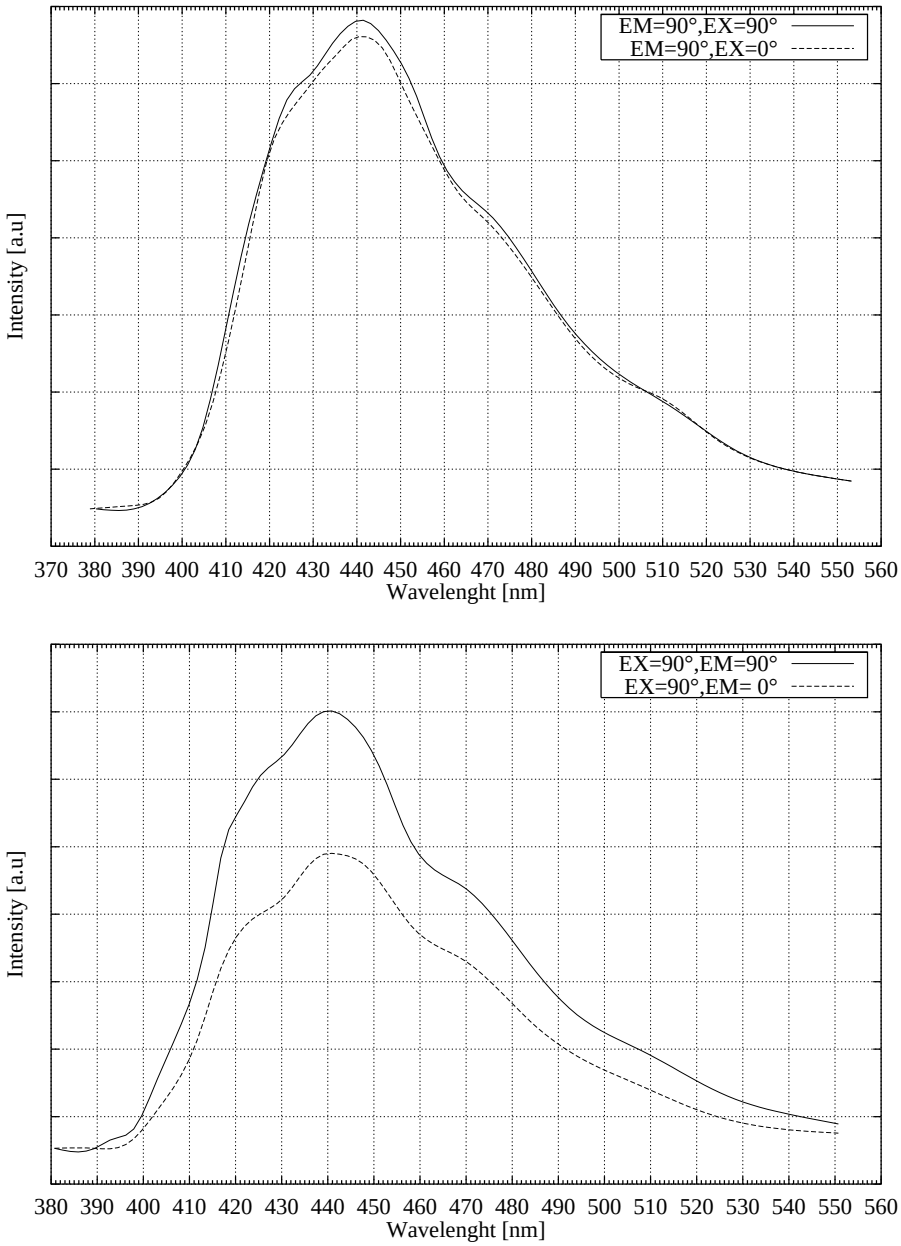

FIGURE 4.43. Sample: gl018; polarized luminescence of PHP in geometry b)

4.2. Polarized photoluminescence on PHP/C_{60} multilayer on glass. A series of PHP/C_{60} multilayer on glass were prepared. On the most samples no luminescence could be detected and was completely quenched due to the electron-transfer to C_{60}. As on PHP-films on glass, the luminescence show a strong anisotropic effect. Fig.4.44 and 4.45 show the action and luminescence spectra of sample multi38. Both spectra were recorded in geometry b.). In geometry a.) no signal was detected. The growth conditions were:

TABLE 4.43. Growth parameter of PHP/C_{60} multilayer

Sample-Nr.	Substrate-material	T_S [°C]	$T_{Wall/Source}$ PHP/C_{60}	Preheat [°C]
multi38	glass	140	240/400	140

The growth times are: 30 min PHP, 20 times (5 min C_{60} / 10 min PHP),5 min C_{60}
Estimated layer thickness of PHP around 30 nm and C_{60} around 20 nm.

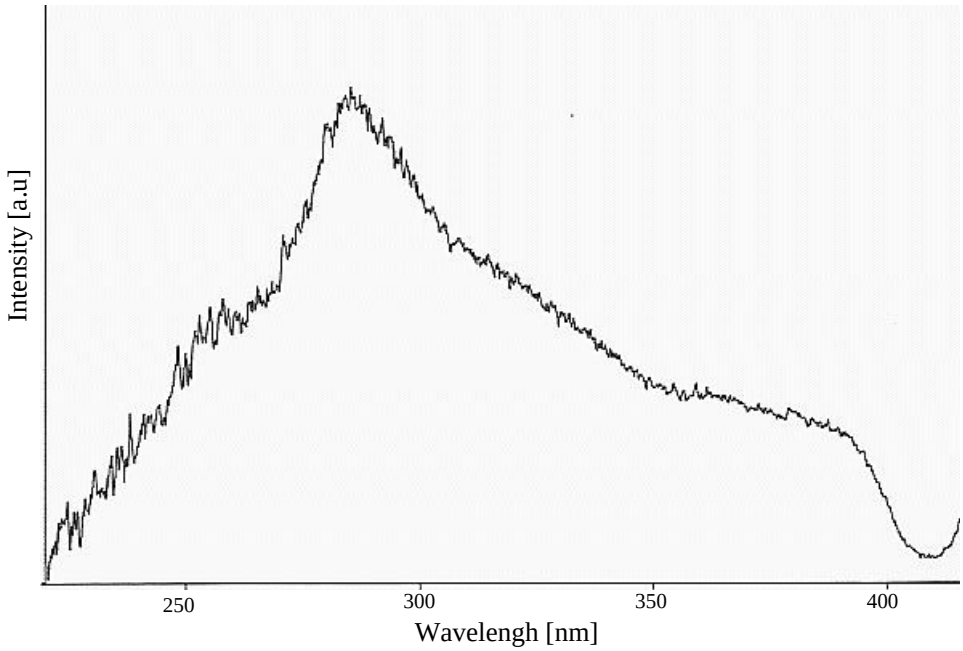

FIGURE 4.44. Sample: multi38. Action spectrum of PHP/C_{60} multilayer in geometry b.). Emission=420nm

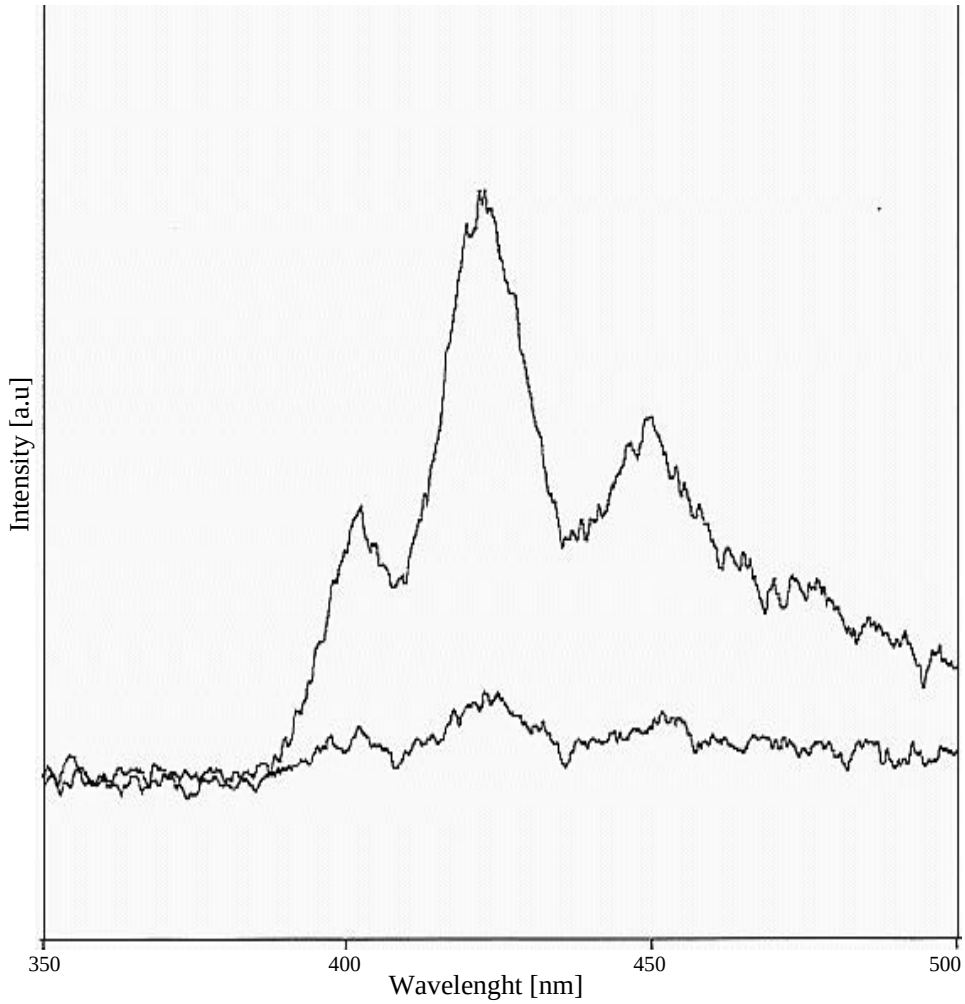

FIGURE 4.45. Sample: multi38. Photoluminescence spectrum of PHP/C_{60} multilayer in geometry b.). Very weak signal EM=90°(bottom spectra) and EM=0°(top spectra). Excitation-wavelength=300nm

5. Photocurrent studies

Molecular crystals of un-doped conjugated polymers have very low intrinsic conductivities. The energy gap of PHP is 3eV, the fraction of electrons exited across the gap at room temperature is of the order of 10^{-27}! This low intrinsic conductivity has dramatic consequences for the description of the metal-oligomeric semiconductor junction as well for the organic hetero-junction interface [**13**].

- At metal/oligomer junction is a negligible charge exchange ocures and the extend of charge region and the band bending is very small
- At the oligomer/C_{60} hetero-junction, there are no charge carriers available to flow across the interface at room temperature. This implies that the depletion layer is very thin (few mono-layers) with nearly vanishing built-in potential
- The metal/oligomer junction can be described as metal/insulator junctions (MIM) rather than metal/semiconductor junction

5.1. PHP and PHP/C_{60} hetero-junction photodiodes. Considering the energy band diagram in fig. 2.1, it is clear that the hetero-junction between PHP and C_{60} should exhibit a rectifing current-voltage characteristics (e.g. analogous to p-n junction). Electron injection (reverse bias) on the C_{60} side from Al contact is energetically unfavorable and results in a very low current density. On the other hand electron injection onto C_{60} from PHP and electron removal from C_{60} to Al is energetically favorable, creating conducting species on both sides.

TABLE 4.45. Growth parameter of PHP/C_{60} films

Sample-Nr.	T_S [°C]	$T_{Wall/Source}$ PHP/C_{60} [°C]	Growth time PHP/C_{60} [min]	Preheat [°C]	Thickness PHP/C_{60} [nm]
dev04	90	240/-	120	90	100
dev05	90	240/400	120/72	90	100/80

In table 4.45 the growth conditions of the organic films are given. Figure 4.47 and fig. 4.48 shows the current voltage characteristics of the ITO-PHP-Al and ITO-PHP/C_{60}-Al device. Positive bias is defined as positive voltage applied to the aluminum contact (reverse bias).

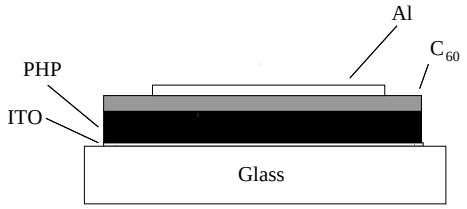

FIGURE 4.46. Schematic cross-section of the hetero-junction devices from PHP and C_{60}

Pure PHP is showing a symmetric current-voltage characteristics, in agreement with the reported absence of rectification in ITO/C_{60}/Au and ITO/MEH-PPV/Al devices [**13, 50**]. Figure 4.48 shows the current-voltage data, with the ITO-PHP/C_{60}-Al device in the dark and with device illuminated with 388nm monochromatic light of a xenon-lamp. Exponentially turn-on up to 0.3 V in forward bias is clearly observable; the rectification ratio is approximately 10^3 and is limited by the ohmic contact of the Cu-wire to Al and ITO contacts respectively (bias $\geq$ 1V). In

fig. 4.49 the spectrally resolved photocurrent of ITO-PHP/ C_{60}-Al device is given. It follows more or less the action-spectrum and absorption of PHP/C_{60} bilayer (see fig.4.50) which initiated the photoinduced electron transfer.

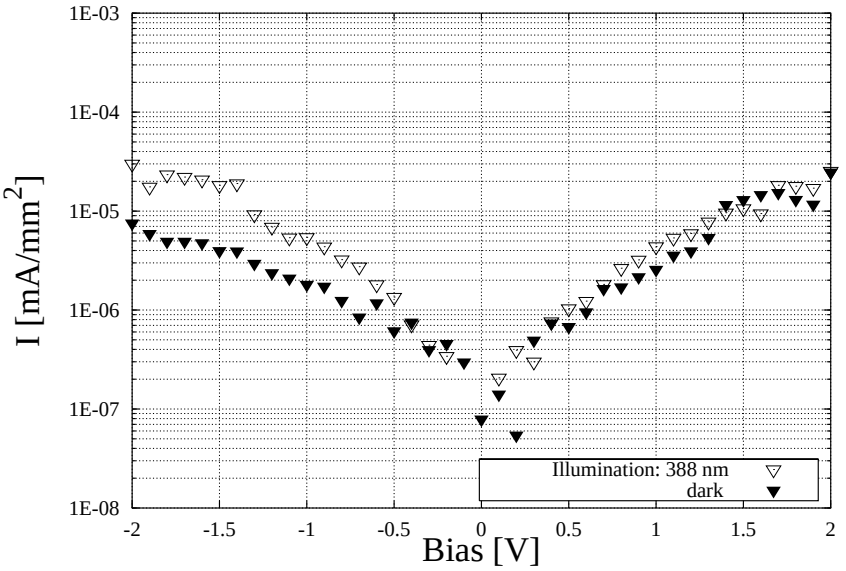

FIGURE 4.47. Sample: dev04. Current vs. voltage characteristics of ITO-PHP-Al device in dark (black triangles) and upon illumination with monochromatic light of a xenon-lamp (open triangles). Intensity=1mW cm^{-2}, Excitation-wavelength=388 nm

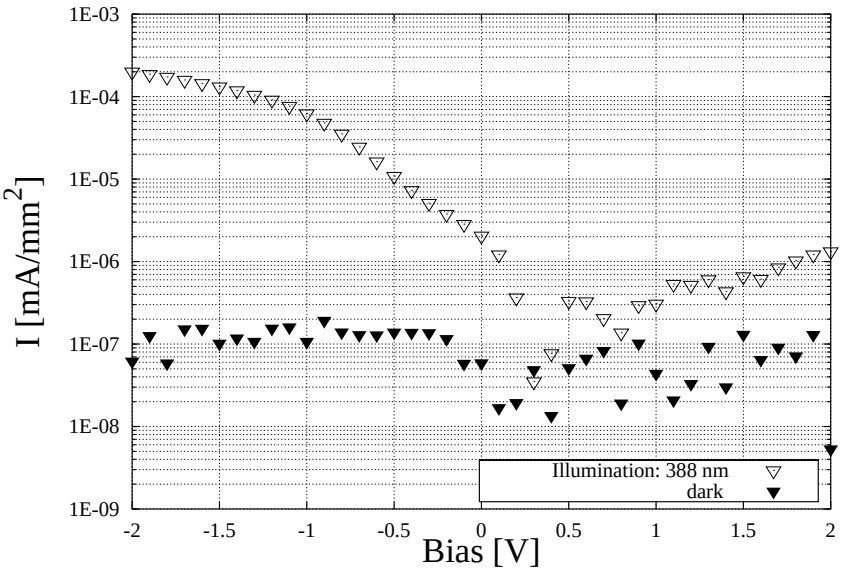

FIGURE 4.48. Sample: dev04. Current vs. voltage characteristics of ITO-PHP/C_{60}-Al device in dark (black triangles) and upon illumination with monochromatic light of a xenon-lamp (open triangles). Intensity=1mW cm^{-2}, Excitation-wavelength=388 nm

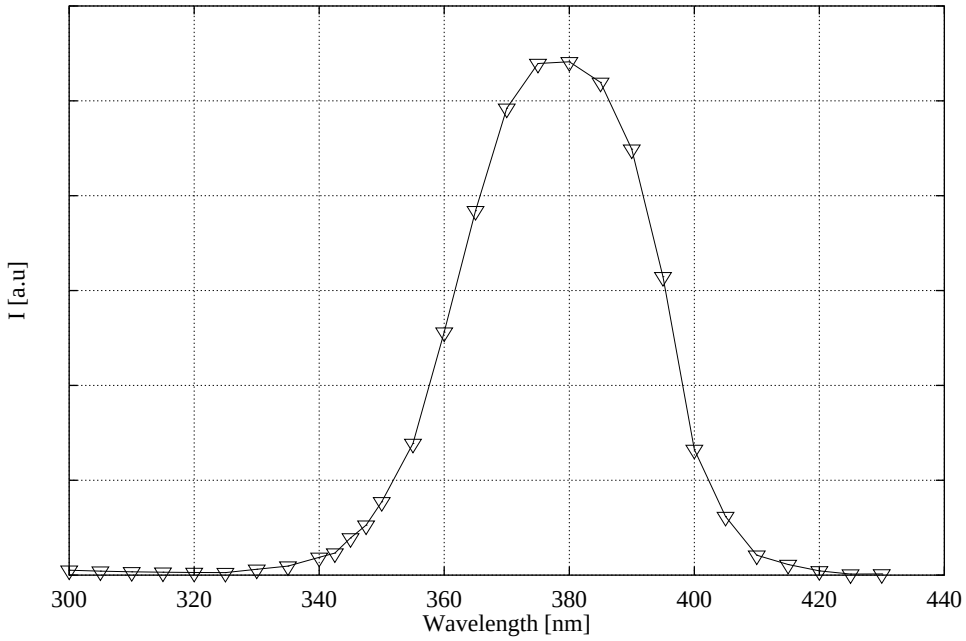

FIGURE 4.49. Sample: dev05. Spectrally resolved photocurrent of ITO-PHP/C_{60}-Al device unter forward bias -2 V. Excitation intensity=1mW cm^{-2} was determined by a calibrated Si-Diode.

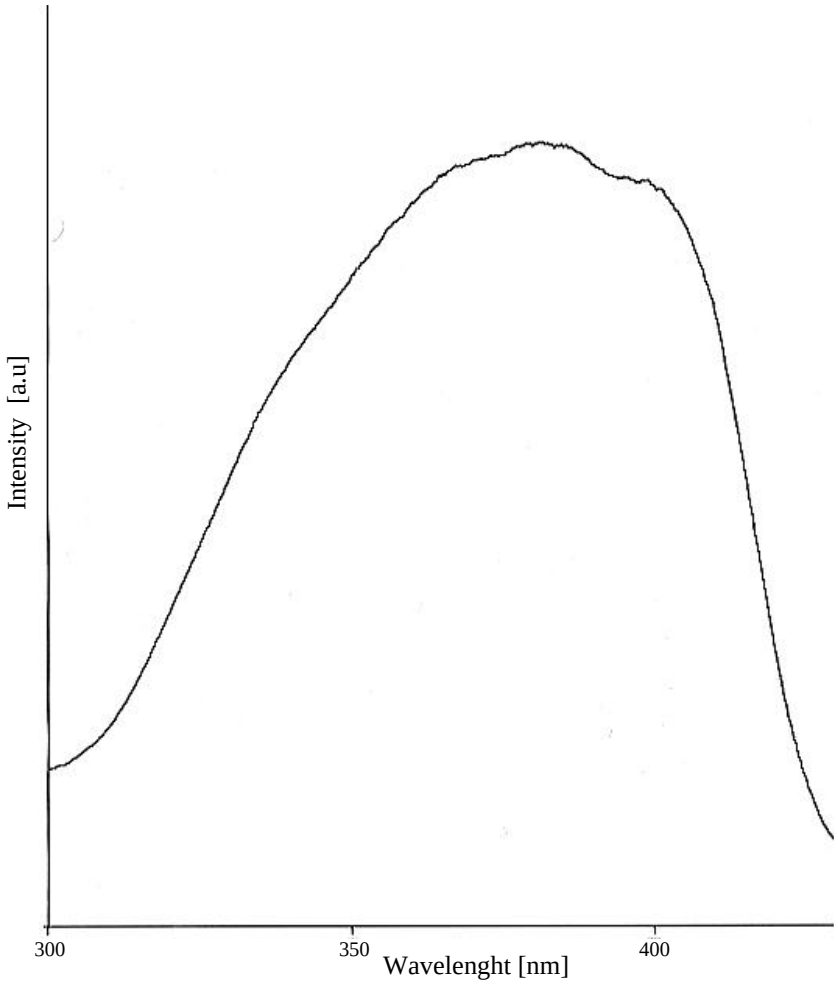

FIGURE 4.50. Sample: dev05. Action spectrum of PHP/C_{60} bilayer on glass. Excitation acts perpendicular to the substrate. Emission is set to 440nm.

Bibliography

[1] D. Stifter and H. Sitter. Hot wall epitaxy of C_{60}-thin films on mica. *Appl. Phys. Lett.*, 66:679, 1995.

[2] D. Stifter and H. Sitter. Herstellung dünner C_{60}-Schichten mittels Hot Wall Epitaxie. Master's thesis, J.Kepler Univ. Linz, 1994.

[3] A. Niko, F. Meghdadi, C. Ambrosch-Draxl, P. Vogel, and G. Leising. Optical absorbance of oriented thin films. *Synthetic Metals*, 76:177–179, 1996.

[4] Denis Fichou, editor. *Handbook of Oligo- and Polythiophenes*. Wiley-VCH Verlag GmbH, D-69469 Weinheim, 1999.

[5] F. Mehdadi, S. Tasch, B. Winkler, W. Fischer, F. Stelzer, and G. Leising. Blue electroluminescence based on para-hexaphenyl. *Synth. Met.*, 85:1441–1442, 1997.

[6] K.N. Baker et al. Crystal structures, phase transitions and energy calculations of ploy(p-phenylene) oligomers. *Polymer*, 34:1571–1587, 1993.

[7] F. Momicchioli, M. C. Bruni, and I. Baraldi. Fluorescence and absorbtion spectra of ploy phenyls: Theoretical study on the band shape. *Jour. Phys. Chem.*, 76:3983–3990, 1972.

[8] P. Atkins. *Physical Chemistry*. Oxford University Press, 1990.

[9] K. Seki, U. O. Karlsson, R. Engelhardt, E. E. Koch, and W. Schmidt. Intramolecular band mapping of poly(p-phenylene) via uv photoelectron spectroscopy of finite ploy phenyls. *Chem. Phys*, 91:459–470, 1984.

[10] Renè and A.J. Janssen. *Primary Photoexcitation in conjugated polymers Chapter 18: Photoexcitation in conjugated oligomers*. World Scientific Publishing Co. Pte. Ltd., PO Box 128, Farrer Road, Singapore 912805, 1997.

[11] Mark G. Harrison and Richard H. Friend. *Handbook of Oligo- and Polythiophenes Chapter 8: GranströmElectro-optical Polythiophene Devices*. Wiley-VCH Verlag Gmbh, D-69469 Weinheim, 1999.

[12] C. Taliani and W. Gebauer. *Handbook of Oligo- and Polythiophenes Chapter 7: Electronic Exited States of conjugated Oligothiophenes*. Wiley-VCH Verlag GmbH, D-69469 Weinheim, 1999.

[13] N. S. Sariciftci, L. Smilowitz, A. J. Heeger, and Wudl. *Sience*, (258):1474, 1992.

[14] N. S. Sariciftci and A. J. Heeger. *Int. J. Mod. Phys.*, B 8(237), 1994.

[15] N. S. Sariciftci. *Prog. Quant. Electr*, (19):131, 1995.

[16] N.S. Saricifci and A. J. Heeger. *Handbook of Organic Conductive Molecules and Polymers*. John Wiley & Sons, 1997.

[17] X. Wei, Z. V. Vardeny, N. S. Sariciftci, and A. J. Heeger. *Phys. Rev. B*, (53):2187, 1996.

[18] G. Yu, J. Gao, J. C. Hummelen, F. Wudl, and A. J. Heeger. *Science*, (270):1789, 1995.

[19] N. S. Sariciftci, D. Braun, C. Zhang, V. Srdanov, A. J. Heeger, G. Stucky, and F. Wudl. *Appl. Phys. Lett.*, (62):585, 1993.

[20] K.Yoshino, X. H. Yin, S. Morita, T. Kawai, and A. A. Zakhidov. *Sol. State Commun*, 85(85), 1993.

[21] S. Morita, A. A. Zakhidov, and K. Yoshino. *Sol. State Commun*, (82):249, 1992.

[22] B. Horowitz. *Solid State Commun*, (41):729, 1982.

[23] L. Smilowitz and A. J. Heeger. *Synth. Met.*, (48):193, 1992.

[24] G. Zerbi, M. Gussoni, and C. Castilioni. *Conjugated Polymers*. Kluwer Academic Publ., Dordrecht, 1991.

[25] K. H. Lee, R. A. J. Janssen, N. S. Sariciftci, and A. J. Heeger. *Phy. Rev. B*, (49):5781, 1994.

[26] J. W. Arbogast, A. O. Darmanyan, C. S. Foote, Y. Rubin, F. N. Diederich, M. M. Alvarez, S. J. Anz, and R. L. Whetten. *J. Phys. Chem.*, (95):11, 1991.

[27] C. Brabec et al. *accepted for publication by J. Chem. Phys.*, 1998.

[28] V. Dyakonov et al. *submitted to Phys. Rev. B.*, 1998.

[29] G. Dellepiane, C. Cuniberti, D. Comoretto, G. Lanzani, G. F. Musso, P. Piaggio, R. Tubino, A. Borghesi, C. Dell'Erba, G. Garbarino, and L. Moramarco. *Phys. Rev. B*, (45):6802, 1992.

[30] H. Meier. *Organic Semiconductors*. Verlag Chemie, Weinheim, 1974.

[31] C. W. Tang. *Appl. Phys. Lett.*, 48:183, 1986.

[32] J. B. Whitlock, P. Panayotatos, G. D. Sharma, M. D. Cox, R. R. Sauers, and G. R. Bi. *Optical Engineering*, (32):1921, 1993.
[33] B. Ot'Regan and M. Gratzel. *Nature*, (353):737, 1991.
[34] W. A. Nevin and G. A. Chamberlain. *IEEE Transaction on Electron Devices*, (40):75, 1993.
[35] J. Kanicki. *Conducting Polymers*. Marcel Dekker, New York, 1986.
[36] G. Horowitz. *Adv. Mater.*, (2):287, 1990.
[37] K. Uehara, A. Maekawa, A. Sugimoto, and H. Inoue. *Thin Solid Films*, (215):123, 1992.
[38] Y. Yamashita, W. Takashima, and K. Kaneto. *Jpn. J. Appl. Phys.*, (32):L1017, 1993.
[39] A. Lopez-Otero. *Thin solid Films*, 49:3–57, 1978.
[40] H. Sitter, D. Stifter, and T. Ngyen Manh. Preparation of pristine and ba-doped C_{60} films by hot-wall epitaxy. *Journal of Crystal Growth*, 174:828–836, 1997.
[41] H.Sitter, D. Stifter, and T. Ngyen Manh. *Molecular Nanostructures: Electronic transport in single crystal Ba_xC_{60} films by hot-wall epitaxy*. World Scientific, Kirchberg Tirol, 1997.
[42] W. Faschinger. PhD thesis, Univ. Linz, 1989.
[43] R. Resel, N. Koch, F. Meghdadi, G. Leising, W. Unzog, and K. Reichmann. Growth and preferred crystallographic orientation of hexaphenyl thin films. *Thin Solid films*, 305:232–242, 1997.
[44] R. A. J. Janssen, L. Smilowitz, N. S. Sariciftci, and D. Moses. Triplet-state photoexcitation of oligothiophene films and solutions. *J. Chem Phy.*, 101:1787–1797, 1 August 1994.
[45] A. Yassar, G. Horowitz, P. Valat, V. Wintgens, H. Hmyene, F. Deloffre, P. Srivasta, P. Lang, and F. Garnier. *J. Phys. Chem*, 99:9155–9159, 1995.
[46] A. Yassar, P. Valat, V. Wintgens, H. Hmyene, F. Deloffre, G. Horowitz, P. Srivasta, and F. Garnier. *Synth. Met*, 67:277–280, 1994.
[47] F. Deloffre, F. Garnier, P. Srivasta, A. Yassar, and J. L. Fave. *Synth. Met*, 67:223–226, 1994.
[48] L. Athouel, J. Wery, B. Dulieu, J. Bullot, J. P. Buisson, and G. Froyer. Optical properties of polyparaphenyl thin films from oligomers to polymers. *ICSM*, (4010):287–288, 1996.
[49] R. N. Marks, M. Muccini, E. Lunedi, R. H. Michel, M. Murgia, R. Zamboni, C. Taliani, G. Horowitz, F. Granier, M. Hopmeier, M. Oestreich, and R. F. Mahrt. Disorder infuluenced optical prperties of α-sexithiophene single crystals and thin evaporated films. *Chem. Phys.*, 227:49–56, 1998.
[50] H. Yonehara and C. Pac. *Appl. Phys.*, 75:539, 1992.